2012

Iron Molybdenum Cofactor: Catalyst In Dihydrogen Production And Nifen's Role In The Femo-co Biosynthetic Pathway

Deborah Bolin Maxwell
University of Central Florida

IRON-MOLYBDENUM COFACTOR: CATALYST IN DIHYDROGEN PRODUCTION AND ROLE OF NIFEN IN THE FEMO-CO BIOSYNTHETIC PATHWAY

by

DEBORAH BOLIN MAXWELL
M.S. University of Central Florida, 2007
B.S. University of Central Florida, 1978

A dissertation submitted in partial fulfillment of the requirements
for the degree of Doctor of Philosophy
in the Department of Chemistry
at the University of Central Florida
Orlando, Florida

Summer Term
2012

Major Professor: Robert Y. Igarashi

ABSTRACT

Humankind's tremendous industrial and technological progress over the last two centuries has been driven by the natural abundance and availability of fossil fuels. As those reserves deplete, the prudent course of action would be to develop other readily available fuel sources. Some research efforts using biomolecules involve the hydrogenases and nitrogenases with the goal of evolving dihydrogen. At the nitrogenase active site, the iron-molybdenum cofactor (FeMo-co) catalyzes the reduction of dinitrogen and protons to form ammonia and dihydrogen.

Toward the goal of producing dihydrogen passively as an alternative fuel, a novel advanced material has been developed. CdSe nanoparticles complexed with FeMo-co, in both aqueous and organic solvent systems showed complex formation. When the system was interrogated by EPR spectroscopy, evidence of electron transfer was observed. The CdSe-MSA●NafY●FeMo-co system when illuminated with visible light evolved dihydrogen consistently in four different experimental sets under the same reaction conditions.

NifEN protein plays an important role in the biosynthesis of FeMo-co in addition to the involvement of NifU, NifS, NifB, NifX, NifH and NafY. After NifB synthesizes a FeMo-co precursor, 6-Fe NifB-co, NifEN further incorporates additional Fe, S, Mo, and (*R*)-homocitrate to complete the synthesis of FeMo-co. Molybdenum is provided to NifEN as its oxoanion, $Mo(VI)O_4^{2-}$; however, in FeMo-co molybdenum is in the oxidation state of Mo(IV). EPR spectroscopic investigation of NifEN turnover samples showed a signal at $g = 2.00$ that was dependent on molybdate concentration. Power and temperature profiles gave evidence that the *g*

= 2.00 EPR signal was distinct from the Fe-S clusters in NifEN. The species observed at g = 2.00 was assigned to the reduction of Mo(VI) to Mo(V).

How to utilize the effectiveness of FeMo-co and complex it to photoactive materials for the purpose of evolving dihyrogen upon illumination, thus providing a sustainable alternative energy source is one subject of this dissertation. A related subject is to gain an understanding of the biosynthetic pathway of FeMo-co by investigation of NifEN turnover experiments. This understanding should contribute towards the development of improved catalysts for meeting future energy demands.

I have a wonderful family who has been my constant support. Their understanding and patience have been inestimable. I would like to dedicate this dissertation to Michael, my husband and friend, along with his father and mother, Robert and Alice. I also dedicate this work to our family Jessica, Nick, Brent, Ricardo, Frances, Isaac, Jacqueline, Daniel, Jonathan, Libby and Joseph. I further dedicate this work to my father, Junius T. Bolin and his wife Betty Ann. I especially appreciate my brother and his wife and this dedication includes them, Ted and Tracey Bolin, and my nephews Bryce and Christopher, along with their brother, Brent who is in heaven. And one last but not least dedication is to my mother who left us for a better place in 2009. Thank you, Mom. I miss you.

ACKNOWLEDGMENTS

No one can attain a graduate degree without the guidance and help from a number of people. I would like to express my gratitude to Dr. Robert Y. Igarashi who has been my advisor. He has taught me well and prodded me to improve in so many ways. His love for the scientific method and thirst to explore ways to improve the lot of humanity through developing alternative energy sources are inspirational.

I would like to thank all that served on my dissertation committee. Your insights have been very beneficial. I am indebted to Dr. Dmitry Kolpashchikov, Dr. Stephen Kuebler, Dr. William Self and Dr. Cherie Yestrebsky. I appreciate your help in guiding and assisting me in the path towards graduation. I especially am grateful to Dr. Andres Campiglia for his guidance and kind assistance.

Others have certainly contributed to my understanding of the Chemistry behind my project for which I offer my appreciation. Their enthusiasm for science is contagious. I owe a special debt of gratitude to Dr. Namrata Singh, Dr. Alicja Copik, Dr. Kevin Belfield, Dr. Christan Clausen, Dr. Masahiro Ishigami, Dr. Alexander Angerhofer, Dr. CiceronYanez, Dr. Andrew Frazer, Dr. Pedro Marin Patino, Dr. Gerald Mattson, Dr. D. Howard Miles, Dr. David Richardson and Dr. Jingdong Ye.

My labmates are truly mates. They have challenged me to strive towards excellence. I am grateful for the opportunity to work with so many talented people. Many thanks to Jirair Gevorkyan, Lynn Sims, Finoa Zullo, Brian Tish, Brett Fleisher, Marilyn Mosquera, Heather Burke, Heena Ahmed, Mitchell Barnes, Matthew Dickens, Tayler Croom, Demi Vasilatis, Christopher Radka, Allyssa Miller, Matthew Szasz, Jason Meeks, and Matthew Weber.

TABLE OF CONTENTS

LIST OF FIGURES

LIST OF TABLES

CHAPTER ONE: INTRODUCTION

Fossil Fuel Reserves are Finite and are Being Rapidly Depleted

Humankind's tremendous industrial and technological progress over the last two centuries has been driven by the natural abundance and availability of fossil fuels. The news is not welcomed, but the world's nations are long overdue in developing renewable energy sources to a level that could approach or match the current use of any of the fossil fuels. Within one generation, all petroleum reserves may be depleted. Each year, eighty-six percent of all energy consumed worldwide comes from fossil fuels. At current usage levels, the estimated years left of petroleum reserves are 47 years; natural gas reserves are 60 years and coal reserves are 131 years (*1*).

Presently, six percent of energy consumed annually comes from renewable energy sources, which include solar, wind, geothermal and hydroelectric categories. Solar energy is accessed by solar cells, which provide 0.1% of electric current used in the United States. Other countries such as Germany, South Korea and Israel utilize solar cells at greater percentages, but nothing yet as to match the use of fossil fuels (*2*).

An important aspect of energy use that has greatly contributed to humankind's advancement and development is the Haber-Bosch process. For almost 100 years Fritz Haber's method to produce NH_3 from molecular hydrogen and nitrogen, which was scaled up and commercialized by Carl Bosch, has provided synthetic fertilizers to world-wide agriculture and raw materials for industry. The estimate is that 40% of the world population's nutrition originates with the Haber-Bosch process (*3*) .

Haber-Bosch uses an iron catalyst and the energy intensive conditions of 300 to 500° C, and 200 to 300 atmospheres of pressure. Approximately 1 to 2 % of world annual energy consumption is estimated to be directed towards the Haber-Bosch process. Some improvements such as adding potassium to the iron's surface have been made to the catalyst to improve efficiency. However, the industrial process remains much the same as originally formulated prior to World War I (*4*). Nitrogen fertilizers have certainly been beneficial for humanity. However, there is a downside to their use such as the eutrophication of waterways, which has resulted in fish kills and unhealthy ecosystems.

Research Focused on Use of Solar Energy to Generate Alternative Energy Sources

Currently, the best known method for accessing solar energy is the solar cell. However, there are other adaptations accessing solar energy for generating a clean source of energy. A water splitting material that produces dihydrogen and dioxygen when illuminated with ultraviolet light, titanium oxide, used mostly in fuel cells, has been a major research area for three decades (*5*). Research efforts have focused on forming composites with TiO_2 to enable visible light to perform water splitting with some limited success (*6*). Another research area showing promise is the artificial leaf, a silicon sheet coated with a cobalt based catalyst on one side and nickel-molybdenum-zinc alloy layer on the opposite side. When this silicon composite is illuminated with visible light and immersed in water, it evolves dihydrogen and dioxygen in appreciable amounts (*7*, *8*).

A major research effort using biomolecules to generate dihydrogen as an alternative fuel source focuses on the use of hydrogenases. These enzymes found in microorganisms catalyze

the formation of dihydrogen from available protons and many of the hydrogenases also perform the reverse reaction to oxidize dihydrogen (*9*). Nitrogenase found in diazotrophs also catalyzes the formation of dihydrogen, but its major function is to perform nitrogen fixation, making the element nitrogen bioavailable in the form of ammonia and/or downstream nitrogen containing metabolites (*10*). Nitrogenase, however, in the absence of the substrate dinitrogen, will catalyze the formation of dihydrogen from protons (*11*).

Recent reports that produce dihydrogen by bioconjugate methods include the following examples. Self-assembled complexes between cadmium telluride nanocrystals and Fe-Fe hydrogenase from *Clostridium acetobutylicum* when illuminated with a visible light source have produced dihydrogen with ascorbic acid serving as an electron donor (*12*). A NiFeSe-hydrogenase from *Desulfomicrobium baculatum* complexed with ruthenium dye-sensitized TiO_2 was illuminated either with a tungsten halogen lamp or with sunlight and was effective for production of dihydrogen (*13*). A molybdenum-iron protein (MoFe protein), component I protein of nitrogenase, was conjugated with $Ru(bypy)_2$ near the catalytic site. When the complex was illuminated with a xenon/mercury lamp and provided with the substrates of protons or acetylene, the system produced the corresponding reduced products of dihydrogen and ethylene (*14*).

In looking for solutions to develop a reliable and sustainable effort to generate dihydrogen from solar energy and for development of new and improved catalysts to fix nitrogen to feed the world's population, perhaps a wise choice to probe is the use of one of Nature's best catalysts, the iron-molybdenum cofactor (FeMo-co) of nitrogenase. FeMo-co could be complexed to a photo-active material. Electron transfer to FeMo-co could be facilitated and

thereby reduce protons to form dihydrogen. Furthermore, elucidating the biosynthetic pathway to form FeMo-co could lead toward development of a better novel catalyst for industrial production of NH_3 and could also lead to biomimetic systems that would generate dihydrogen. Both areas could contribute to developing new energy resources that would have fewer negative impacts on the environment. In order to access this advantageous catalyst from Nature, a way to deliver electrons must be determined.

Cadmium Selenide Nanoparticles and their Use as Photoactive Materials

Nanotechnology has been at the forefront of developing new materials for applications in electronic, biological and medical arenas. CdSe n-type semi-conductor quantum dots, one of numerous nanoparticle materials, exhibit size tunable optical properties related to their band-gap energy (*15, 16*). Band gap energy is defined as a semiconductor's threshold energy necessary for absorption of photons (*17*). The variation of nanoparticle size also results in energy of luminescence light emitted from photo-excited nanoparticles (*18*). The variation in size of quantum dots exhibits changes in coloration as long as the quantum dot radius is within their Bohr exciton radius (5.6 nm for CdSe). This effect is due to quantum confinement, which is a strong confinement of electrons and their holes as observed relating to their light-matter interactions (*19*).

Quantum confinement in quantum dots can be further described as strong three-dimensional confinement of excitons that exceed coloumbic attraction. The small surface-to-volume ratios of these nanoparticles contribute to their size tunable properties. Upon photo-activation, excitons in the quantum dots will cool and relax within the intra-band region at the

rate of 10^{11} s^{-1}. Next, inter-band recombination occurs in one of the following ways: radiative relaxation at the band edge, non-radiation relaxation arising from phonons, or Auger non-radiative relaxation and non-radiatitve relaxation at the surface defects (*19*). The excited electron will relax as described unless an adsorbed surface species quickly accepts the electron in an electron transfer event. Smaller nanoparticles lessen the recombination probability, because the distance that the excited pair, electron and hole, have to migrate to surface sites is decreased resulting in enhanced photo-activity (*6*).

The relaxation process of radiative exciton recombination at the band edge and deactivation of excited electrons (holes) at the surface states are responsible for the size-tunable photoluminescent colors of different sized CdSe quantum dots. In CdSe quantum dots, the exciton recombinations at the band edge are transitions from 5*s* orbitals of Cd in the lowest unoccupied molecular orbital (LUMO), combined with 4*p* orbitals of Se in their highest occupied molecular orbital (HOMO). The second source of photoluminescence in quantum dots is the surface state deactivation of excited electrons (holes). Both of these inter-band relaxations occur relatively slowly, $< 10^{9}$ s^{-1} and at a non-exponetial rate caused by carrier trapping at shallow surface defects (*19*).

When a CdSe nanoparticle is illuminated, an excited electron in its valence band will move to the conduction band if the incident radiation is of high enough energy to match or exceed the band gap energy. If this excited electron is going to participate in electron transfer, then a sacrificial electron donor needs to be present to fill the electron hole in the valence band after the electron is excited to the conduction band. The presence of the electron donor is necessary to maintain charge neutrality. With adequate charge separation in high quality

quantum dots, electrons may be available for electron transfer to an adsorbed species on the CdSe nanoparticle surface (*6, 20*). If this surface adsorbed species is a catalyst with a negative enough reduction potential then it could possibly perform a proton reduction (Figure 1). CdSe nanoparticles have a band gap energy of 1.7 eV, which is close to the thermodynamics for the H^+/H_2 couple at pH of 7 (Equation 1).

$$2\ H^+ \ + \ 2\ e^- \ \rightarrow \ H_2 \quad E° = -0.47\ V\ (NHE)\ pH\ 7 \quad (Eq.\ 1)$$

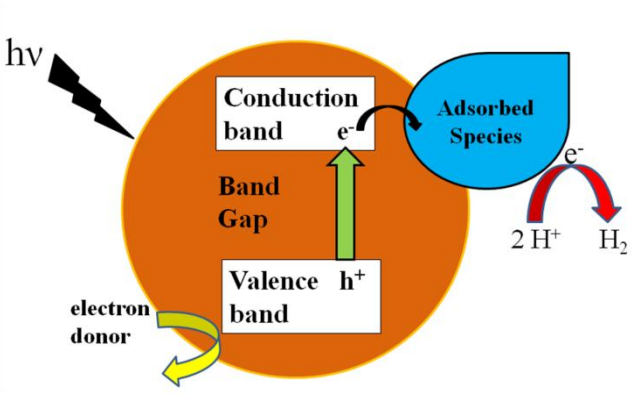

Figure 1. A Photo-excited CdSe Nanoparticle that Performs an Electron Transfer to an Adsorbed Species that Catalyzes Dihydrogen Production.

To produce photo-active CdSe nanoparticles, careful attention to synthesis is required. The first reported synthesis of CdSe nanoparticles was a 230-300 ºC pyrolysis of organometallic precursors, dimethyl cadmium and selenium with organic solvent trioctylphosphine and/or the reagent, trioctylphosphine oxide (*21*). Later, a less toxic alternative synthesis was developed replacing the dimethyl cadmium with cadmium oxide. Additionally, the use of trioctylphosphine as a capping agent and phosphonic acids allowed for slowing of the growth and better control of

the nanoparticle size (*22*). Nanoparticles of high quality that are monodispersed in size distribution (~ 30 nm FWHM) have higher photo-activity and luminescence characteristics (*19*). CdSe nanoparticles utilizing this type of synthetic strategy with such capping agents are soluble in organic solvents such as hexane, octadecene or chloroform.

A further adaptation in the synthetic strategy allows for a slowing of nanoparticle growth and more control to achieve targeted sizes. By including tetradecylphosphonic acid in the selenium reagents prior to addition to the cadmium oxide reagents at a specific temperature this allows for a consistent production of 2.4 nm diameter CdSe quantum dots at a set time of reaction due to the enhanced manageability of the synthesis procedure (*23-25*).

Cadmium selenide with trioctylphosphine surface functionalized quantum dots in organic solvents are well known for their photo-activity, but this precludes their use in many biological applications due to their aqueous incompatibility. Cadmium selenide nanoparticles can also be synthesized and processed to allow aqueous solubility. Aqueous soluble quantum dots can be synthesized by several routes that include: a direct synthesis method by an arrested precipitation technique in aqueous media(*26*); by encapsulating the organically soluble quantum dot in a polymerized silica shell functionalized with polar groups or an amphilphilic polymer coating that can significantly add to the quantum dot diameter (*27*); or by replacement of the capping agent on the nanoparticle from trioctylphosphine or trioctylphosphine oxide with a mercapto-carboxylic acid (*28*). Of the mercapto-carboxylic acids, mercaptosuccinic acid was reported for its enhanced luminescence compared to other capping agents (*29*) .

Iron-Molybdenum Cofactor: the Reductive Catalyst at the Active Site in Nitrogenase.

The energy intensive reduction of dinitrogen (N_2) to form ammonia (NH_3) and hydrogen (H_2) as a co-product is performed by diazotropic microbes that utilize the metalloenzyme nitrogenase. A significant portion of microbial nitrogen fixation is performed by the symbionts, *Rhizobia*, typically found on legume root nodules; however, the majority of nitrogen fixation is performed by cyanobacteria on the surface of the earth's oceans (*11*). The free-living diazotrophic soil bacteria are more easily cultivated for scientific study, two of which are *Azotoabacter vinelandii* and *Klebsiella pneumoniae*. Other categories of diazotrophs are various archaea, cyanobacteria and the purple photosynthetic bacteria (*30*).

The most prevalent form of nitrogenase contains molybdenum and iron and consists of two component proteins, MoFe protein, Component I, identified as dinitrogenase, and Fe protein, Component II, known as dinitrogenase reductase, that contain three Fe-S clusters distributed in the two component proteins (Figure 2). The Fe protein, a homodimer, has a Mg-ATP binding site in each subunit and one Fe_4S_4 cluster between the two subunits. This inter-subunit Fe_4S_4 cluster in the Fe protein is coordinated by two cysteines from each subunit (*31*).

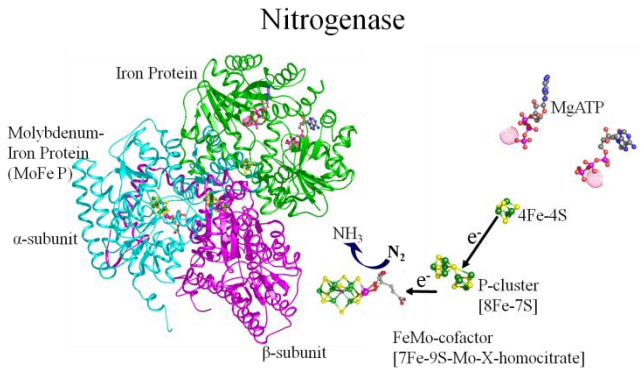

Figure 2. Component Proteins of Nitrogenase with Path of Electron Transfer to FeMo-co. MoFe and Fe protein components of nitrogenase are shown with the pathway for electron transfer starting with Mg-ATP hydrolysis, continuing to the P-cluster and arriving at FeMo-co.

The heterotetrameric MoFe protein has an α and β subunit arranged as dimers of dimers, $\alpha_2\beta_2$, with internal *C*2 symmetry between each αβ dimer. Each α subunit binds a single FeMo-co cluster. The second type of Fe-S cluster in MoFe protein, the Fe_8S_7 P-cluster appears to mediate electron transfer between the transiently associated Fe and MoFe proteins. The P cluster is bound between each interface of the α and β subunits.

FeMo-co is positioned at the active site in the MoFe protein, where nitrogen reduction occurs (9). FeMo-co is comprised of two internal cubanes, with seven irons, nine sulfurs, one molybdenum, a homocitrate and an atom, recently identified as a carbon (*32*), at the center of the two cubanes (Figure 3). Coordination within the protein is at the terminal iron to a thiolate of cysteine (α-275^{Cys}) and at the molybdenum to ε-N of histidine (α-442^{His}) (numbering for *A.vinelandii* NifD). FeMo-co is approximately 10 Å below the protein surface (*33*).

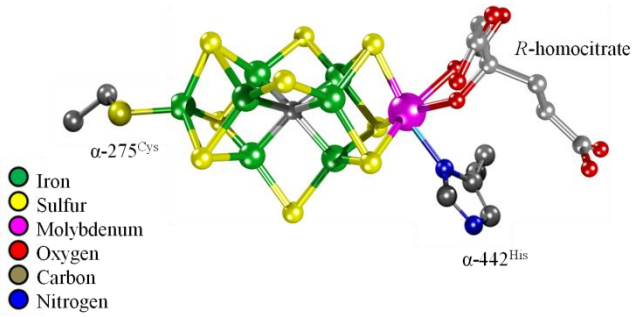

Figure 3. Iron-molybdenum Cofactor (FeMo-co) with Protein Ligands.
Fe_7S_9MoC·*R*-homocitrate is shown with coordinated ligands from the surrounding peptide chain.

The Fe protein containing one Fe_4S_4 cluster and two nucleotide binding sites, couples Mg-ATP hydrolysis to electron transfer to the MoFe protein after docking occurs between the two component proteins. This docking mechanism between the Fe protein and the MoFe protein is followed by a conformational change and appears to trigger the Mg-ATP hydrolysis, leading to the electron transfer to the MoFe protein (34). A single electron, one for every 2 Mg-ATP hydrolyzed, is transferred to the MoFe protein one at a time by way of the P cluster and arriving at the electron's destination, FeMo-co. Substrate binding to FeMo-co does not occur when MoFe protein is in its resting state, but rather occurs only when three or four electrons accumulate. A minimum of 8 cycles of electron transfer, association-dissociation of the complex, must occur in order to facilitate the reduction of N_2 and H^+ to form the products NH_3 and H_2 (Equation 2) (35).

$$N_2 + 8\,e^- + 16\,ATP + 8\,H^+ \rightarrow 2\,NH_3 + 16\,ADP + 16\,Pi + H_2 \quad (\text{Eq. 2})$$

The obligate reciprocal signaling that occurs with each complex association and dissociation event between the Fe and MoFe proteins may be the reason that the Fe protein is the

only known reductant for dinitrogen substrate reduction by the MoFe protein. If no substrate is present, then MoFe protein will reduce protons to form dihydrogen (36) .

FeMo-co that reduces N_2 to form ammonia and protons to form the co-product, H_2, compared to other catalysts is considered to be one of the most reductive catalysts in Nature. Comparison of the reaction conditions in which FeMo-co operates, ambient temperature and pressures, with that of the Haber-Bosch process, 300 to 500° C and 200 to 300 atmospheres of pressure, gives a sense for the catalytic effectiveness of FeMo-co. Novel methods to harness the catalytic capability of FeMo-co to both utililize it directly in a dihydrogen generation system and then to elucidate the secrets of its biosynthesis should contribute toward future development of sustainable energy resources.

Reaction Chemistry with FeMo-co

In 1977, FeMo-co was anaerobically isolated from the MoFe protein into N-methylformamide by an acid extraction procedure. The procedure began with a short acid treatment of the MoFe protein to denature it. The MoFe protein was then precipitated by raising the pH to near its isoelectric point. The precipitated protein was then washed with N-methylformamide, resulting in the extraction of FeMo-co into the solvent NMF solution in a dithionite reduced state. FeMo-co was found to be stable at room temperature. However, it quickly hydrolyzed in aqueous environments (*37, 38*). Acitivity of isolated FeMo-co was analyzed by adding it to an extract of a *ΔnifB* strain, UW 45, to activate the apo-MoFe protein in the extract (*39*). Many studies have investigated chemistry of FeMo-co with various substrates

yielding interesting results that give insight as to FeMo-co's reactivity and catalytic nature as described in the following paragraphs.

FeMo-co was isolated from MoFe protein and observed by EPR and X-ray absorption spectroscopies to have some of the chemical and catalytic properties of MoFe protein This led to the suggestion that dithionite reduced FeMo-co could possibly catalyze N_2 reduction. In further work, the presence of CO, 5-deazaflavin, and EDTA, FeMo-co no longer showed an $S = 3/2$ spin state. The EPR spectrum appeared spin silent. This FeMo-co EPR $S = 3/2$ spin state was diminished in its spin state population. The EPR silent state was not necessarily equivalent to the reduced EPR silent state observed when Fe protein, Mg-ATP and MoFe protein are added together in a reducing dithionite environment suggestive of electron transfer. (*40*)

The addition of chelating agents 1, 10-phenanthroline and 2, 2-bipyridyl to isolated FeMo-co were discussed in a review article relating them to the addition of EDTA to FeMo-co. When 1, 10-phenanthroline was added to dithionite reduced FeMo-co, the intensity of an EPR signal characteristic of a $S = 3/2$ spin state was diminished to an EPR silent state in a reversible reaction. The reason given for this observation was that in the presence of excess dithionite, the neutral ligand replaces an anionic ligand on FeMo-co and thereby decreases its overall charge thus raising its reduction potential. This enables the dithionite to reduce the FeMo-co. To reverse the interaction with 1, 10-phenanthroline, Fe^{2+} was added as compared to the added Zn^{2+} to reverse the reaction with EDTA. Although there are structural similarities between 1,10-phenanthroline and 2,2-bipyridyl, the latter's interaction with FeMo-co did not result in an EPR silent state. Unlike synthetic Fe-S clusters that are completely destroyed by chelating agents, FeMo-co's activity is unaltered by the ligand-exchange reactions (*41*).

To better understand the ligand interaction(s) between extracted FeMo-co and N-methylformamide (NMF), isolated FeMo-co was investigated by FTIR. IR spectroscopy showed that the N-deprotonated amide ligands were bound to FeMo-co at the terminal iron where it binds to cysteine within the protein and at the molybdenum. The binding was different than the typical Fe-S thiolate binding inside the protein. Based on this finding, 2-pyrrolinone was proposed to be able to ligate FeMo-co and indeed was utilized to extract FeMo-co successfully (*42*).

Cyclic voltammetry was used to probe the oxidation states of isolated FeMo-co. FeMo-co was observed to undergo direct electrochemical reduction at a glassy electrode by monitoring with EPR spectroscopy. Chemical redox titrations of FeMo-co demonstrated that FeMo-co can undergo a chemically reversible one electron transfer, evidenced by EPR spectroscopy as a change in electronic spin state, $S = 3/2$ to an integer spin state (*43*).

Another researcher reported a sharpening of the EPR signal when FeMo-co and thiophenol were combined. This thiolphenol treated FeMo-co EPR sharpened signal was much closer in resemblance to the $S = 3/2$ signal seen in MoFe protein as compared to isolated FeMo-co. In a nitrogenase activity assay the thiolphenol treated FeMo-co was shown to be equivalent to the dithionite reduced FeMo-co (*44*).

Isolated FeMo-co was investigated by sulfur K-edge and molybdenum L-edge spectroscopy in the reduced and oxidized states. Other inorganic complexes containing sulfur and molybdenum were also examined by the same spectroscopic technique for comparison. For clear unobstructed observation of the K-edge ionization, the removal of dithionite from the solution was necessary, and the extracted FeMo-co was subjected to an anaerobic

chromatographic procedure before sample preparation. A previously unseen oxidized sulfur with close correspondence to thiolate was observed bound to FeMo-co. By X-ray absorption edge analysis, molybdenum was shown to be in a 4+ oxidation state inside FeMo-co and upon a change in overall oxidation state of FeMo-co, the oxidation state of molybdenum remained unchanged (*45*).

Addition of *p*-$C_6H_4CF_3S$- to FeMo-co and synthetic Fe-S and Fe-Mo-S complexes investigated by ^{19}F NMR demonstrated specific and reversible binding to a single Fe in FeMo-co suggesting that Fe is the most likely thiolate binding site (*46*) Mo K-Edge X-ray Absorption Near Edge Structure (XANES), and Extended X-ray Fine Structure (EXAFS) investigations confirmed this finding. FeMo-co treated with thiophenol and selenol showed identical spectra. Furthermore, EXAFS data with the addition of selenophenol showed that the thiolate binding was on an Fe and not on the molybdenum in FeMo-co (*47*). The demonstrated binding of both thiolate and selenolate species to FeMo-co substantiated the hypothesis that selenide in a nanoparticle could possibly bind to an Fe in FeMo-co.

Isolated FeMo-co was investigated by EXAFS and XANES with further advancements to analyze the EXAFS data. EXAFS showed that a cyanide ligand bound on molybdenum in FeMo-co was possible in the presence of carbon monoxide. Furthermore, the molybdenum was determined to have approximately octahedral geometry and evidence for long-range Mo-Fe-Fe interaction was observed (*48*).

Cyanide and thiols were shown to bind to isolated FeMo-co in its dithionite reduced S = 3/2 spin state and characterized by EPR and magnetic-circular-dichroism (MCD). Cyanide has been found to bind to FeMo-co in more than one site on FeMo-co and causes a perturbation in

the spectra of the dithionite reduced $S = 3/2$ spin state. One of two cyanides bound to FeMo-co can be replaced by a thiol compound such as thiolphenol. A new intense band in the MCD spectrum was observed when the thiolphenol replaced a cyanide, suggestive of a ligand to charge transfer (*49*).

Cyclic voltammetry (CV) has been used to characterize the redox potentials of isolated FeMo-co. A CV measurement showed that when carbon monoxide was added to FeMo-co, the FeMo-co was in an oxidized state. This oxidized state of FeMo-co was reduced back with cyclic voltammetry to obtain the EPR-active state, $S = 3/2$ spin state. Further CV experiments with FeMo-co still bound to carbon monoxide demonstrated two additional reduction steps as observed on the cyclic voltammogram. Purging the system with argon, and thus removing the carbon monoxide, restored the former voltammogram. This FeMo-co was later shown to be active in a nitrogenase assay (*50*).

FeMo-co was extracted into NMF and derivatized by pentafluorothiophenol ($PfpS^-$), on the terminal Fe atom for the purpose of demonstrating that isolated FeMo-co is capable of electro-catalysing the reduction of protons at high potential (-0.28 V). The ligand's function was to be both a ligand to FeMo-co and serve as a source of protons in addition to the water component in the solvent NMF solution. Intially FeMo-co was in the oxidized form, thus EPR was silent. Utilizing cyclic voltammetry, the FeMo-co bound with $PfpS^-$ was reduced by a single electron with the reaction being performed in a sealed electrochemical cell. The headspace was sampled and dihydrogen was detected at the relatively high potential of -0.28 V. The acidity of the $PfpS^-$ (pK_a 2.63), as compared to thiolphenol (pK_a 6.43), was thought to contribute to the

dihyrogen evolution. An enzyme reconstitution assay showed that the FeMo-co was still active and intact (*51*).

Electrochemical and spectroelectrochemical studies of isolated FeMo-co showed that the N-methylfomamide ligand bound to the terminal iron undergoes a rotamerism that is a redox-linked isomerism. The oxidized FeMo-co is observed to undergo three electron reductions. The first two electron transfers were delocalized over the iron-sulfur core of FeMo-co; the third electron transfer event was an irreversible process and was localized on the molybdenum. Spectrochemical studies with ^{12}CO and ^{13}CO demonstrated the binding sites on FeMo-co associated with the electron transfers that gave evidence of the correct assignment of oxidation states in FeMo-co; [$4Fe^{II}3Fe^{III}Mo^{IV}$] in FeMo-co's dithionite reduced state (*52*).

Cyanide binding to isolated FeMo-co was investigated by an electrochemical method and FTIR and EPR spectroscopies. Cyanide was found to coordinate to central iron sites on oxidized FeMo-co, which appeared to increase the electron density on the central iron-sulfur core of the cluster. Furthermore, redox potential for the oxidized state/dithionite reduced couple was altered to a more negative potential such that a new $S = 1/2$ spin state became visible on EPR. The dithionite reduced isolated state of FeMo-co-cyanide is labile. If cyanide alone was bound then proton and substrate inhibition occurred. However, if carbon monoxide was present, then proton reduction was restored for the production of dihydrogen. When both carbon monoxide and cyanide were combined with isolated FeMo-co, vibrational coupling between the two ligands was visible when investigated with FTIR ^{13}C isotopic labeling (*53*).

FeMo-co Biosynthetic Pathway and NifEN's Role in Assembling FeMo-co

Diazotrophic microorganisms containing nitrogenase such *as K. pneumomiae* and *A. vinelandii* have *nif* (nitrogen fixation) and other *nif* accessory genes that code for proteins that comprise nitrogenase itself (NifDK and NifH) or for proteins involved in the FeMo-co biosynthetic pathway. One of the non-*nif* genes is *nafY* (nitrogen accessory factor Y), a gene that codes for a FeMo-co insertase (*54*).

There are at least 12 gene products that participate in FeMo-co synthesis that can be categorized into three groups (Figure 4). The molecular scaffolds are NifU, NifB and NifEN where stepwise assembly of FeMo-co occurs. Additionally, NifB is a SAM radical protein and NifEN is suggested to be a molybdenum reductase. There are metallocluster carriers such as NifX and NafY. NifX transports a FeMo-co precursor to NifEN and NafY transports the completed FeMo-co into *apo*-NifDK. Three enzymes provide substrates for FeMo-co bioassembly. NifS provides sulfur for the initial Fe-S cluster assembled on NifU. NifQ is involved in providing molybdate. NifV, homocitrate synthase, provides homocitrate to NifEN (*54*).

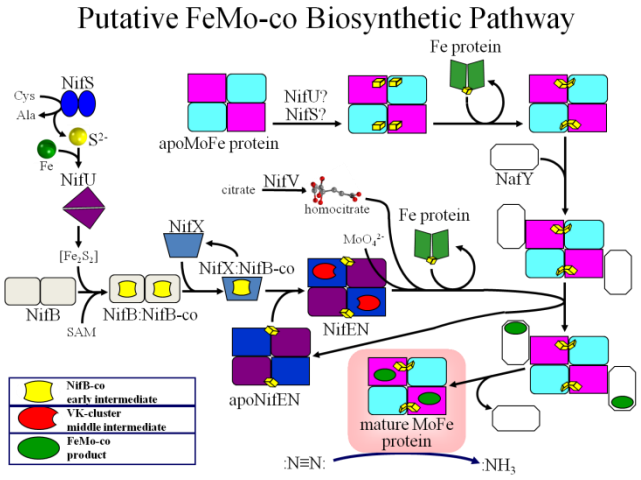

Figure 4. Putative Pathway for the Synthesis of FeMo-co.
NifS provides sulfide to NifU where Fe_2S_2 and Fe_4S_4 clusters are assembled and thereafter provided to NifB, a SAM radical protein. NifB assembles NifB-co that NifX inserts into NifEN. NifEN with the assistance of NifH assembles FeMo-co. FeMo-co binds to NafY that assists with insertion of FeMo-co into the *apo*MoFe protein to form the active species.

The FeMo-co synthetic pathway starts with NifS, which is a cysteine desulfurase that provides sulfide from a cysteine to be combined with Fe to form Fe_2S_2 and Fe_4Fe_4 clusters. These clusters assemble on NifU and are delivered to NifB, which is a SAM radical protein. NifB assembles NifB-co, a FeMo-co precursor, and is most likely a six iron cluster. NifB is also thought to be the likely enzymatic step for the insertion of the carbon central atom. NifX, a carrier of NifB-co, then transports NifB-co to NifEN where the substrates, Mg-ATP, MoO_4^{2-}, homocitrate, Fe and S, all participate in FeMo-co assembly (*54*). NifH most likely is involved in Mg-ATP hydrolysis to facilitate electron delivery. During FeMo-co assembly, homocitrate is incorporated and is thought to stabilize the molybdenum in FeMo-co. The molybdenum in the molybdate oxoanion, MoO_4^{2-}, is in an oxidation state of (VI). This molybdate is the species in which molybdenum is made bioavailable to living organisms. Molybdenum in FeMo-co is in an

oxidation state of Mo (IV). The focus of the research in Chapter 3 is to gain a better understanding of the complicated enzymology that occurs in NifEN, most likely with the assistance of Mg-ATP hydrolysis by NifH, by reducing molybdate for insertion into FeMo-co. NifEN is an $\alpha_2\beta_2$ heterotetramer identified as a scaffold protein because of its significant sequence homology with MoFe protein (*55*).

NafY protein is a 26 kDa chaperone protein that assists with insertion of completely assembled FeMo-co into the *apo*-MoFe protein. It has a high affinity for FeMo-co. From mutagenesis studies, His^{121} in NafY is suggested to bind FeMo-co, which is located on the surface of NafY (*56*). NafY binds independently to FeMo-co or to the *apo*-MoFe protein (NifDK). The presence of NafY has been observed to stabilize *apo*-NifDK, and thereby prepares *apo*-NifDK for FeMo-co insertion (*56*). After the insertion of FeMo-co into *apo*-NifDK, the NafY dissociates from the activated NifDK (*57*).

The EPR spectrum of the NafY•FeMo-co complex is indicative of an $S = 3/2$ spin state that is similar to isolated FeMo-co, but with sharper line shape. The spectrum of the $S = 3/2$ spins state of NafY•FeMo-co complex is similar in appearance to the spectrum of FeMo-co with a ligated thiophenol. Since the EPR spectrum of the $S = 3/2$ spin state is largely similar with that of isolated FeMo-co, the FeMo-co bound to NafY is thought to have similar electronic structure that does not change upon binding to NafY (*56*).

Conclusion

In conclusion, the following studies are presented in this dissertation. First, CdSe nanoparticles and FeMo-co have been combined in both aqueous and organic solvents and

investigated for photocatalytically driven evolution of dihydrogen. Second, the role of NifEN as a molybdate reductase in the biosynthetic pathway of FeMo-co has been investigated.

CHAPTER TWO: PHOTO-ACTIVATED DIHYDROGEN GENERATION BY A CdSe●FeMo-co SYSTEM

Introduction

As the world's need for energy grows, so does the need for developing renewable energy sources. Currently, 15 terawatts (1.5×10^{13} Watts) of energy are consumed worldwide annually, with fossil fuels providing 86% of that energy. The categories of energy forms used each year are 40% petroleum, 23% natural gas, 23% coal, 8% nuclear, and 6% from renewable sources. The projected years left in reserves at the current usage levels are estimated at 47 years for petroleum reserves, 60 years for natural gas reserves and 131 years for coal reserves (*58*). With trade and commerce of energy resources and ecological threats stemming from their use impacting geopolitical stability, the reality is that humankind is at a crossroads, which in turn is driving an imperative to develop alternative energy sources.

Renewable energy sources include solar, wind, hydroelectric and geothermal options. Solar energy is accessed and utilized in several ways. An important way is the use of silicon based solar cells that produces electric current. A recent important breakthrough in the research of inexpensive materials for energy applications is the use of a silicon sheet coated with a cobalt based catalyst on one side and a nickel-molybdenum-zinc alloy layer on the opposite side (*7*). This device, named the artificial leaf, produces notable amounts of dihydrogen and dioxygen when submerged in water and illuminated. Another major current research effort involves the use of TiO_2 exposed to UV radiation which splits water into dihydrogen and dioxygen (*6*). Water-splitting TiO_2 is mostly used in fuel cells that generate electric current from the oxidation of dihydrogen. The challenge over the last three decades has been to develop novel materials to

perform water splitting with energy from the visible light region of the electro-magnetic spectrum. The use of nanoparticles alone or in composite materials with TiO_2 show promise for improving this exploitation of solar energy (*59*).

Another research area toward the goal of accessing solar energy, but with a somewhat different outcome is the production of dihydrogen as an alternative fuel source by utilizing biomolecules. Some of the ways that biological systems produce dihydrogen is by using two enzymes of hydrogenases and nitrogenases found in certain microorganisms. Developing ways to utilize and adapt this dihydrogen generating ability of these enzyme systems can be grouped in three broad approaches of using an enzyme itself; forming a hybrid between different enzyme components and a synthetic material, or by synthesizing a biomimetic analog of the biological catalyst.

There are several published methods that have photocatalytically generated dihydrogen among which these are examples. Self-assembled complexes between cadmium telluride nanocrystals and Fe-Fe hydrogenase from *Clostridium acetobutylicum* when illuminated with a visible light source have produced dihydrogen with ascorbic acid serving as an electron donor (*12*). A NiFeSe-hydrogenase from *Desulfomicrobium baculatum* complexed with ruthenium dye-sensitized TiO_2 was illuminated either with a tungsten halogen lamp or with sunlight and was effective for production of dihydrogen (*13*). An altered molybdenum-iron protein (MoFe protein), component I protein of nitrogenase, was complexed with $Ru(bypy)_2$ near the catalytic site. When the complex was illuminated with a xenon/mercury lamp and provided with the substrates of protons or acetylene, the system produced the corresponding reduced products of dihydrogen and ethylene (*14*). Perhaps a different approach with the goal of photocatalytically

generating dihydrogen could involve the use of the iron-molybdenum cofactor (FeMo-co, Figure 5), which is the catalytic cofactor found in the active site of the molybdenum-iron protein (MoFe protein) component of nitrogenase.

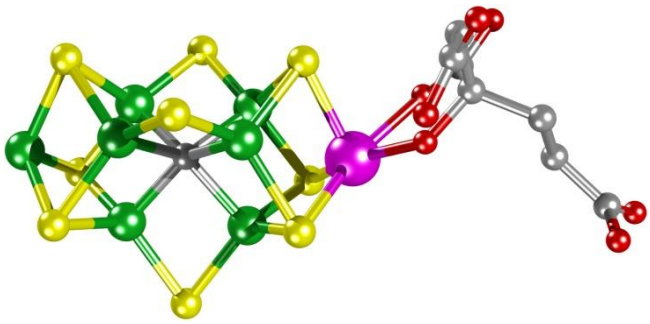

Figure 5. Structure of the Iron-Molybdenum Cofactor (FeMo-co)
The Fe_7MoS_9C-(*R*)-homocitrate cluster is comprised of 7 irons (green), 9 sulfurs (yellow), one carbon (gray), one molybdenum (magenta), and one (*R*)-homocitrate ligand.

Diazotrophic microorganisms utilize nitrogenase to perform nitrogen fixation. The most prevalent and best-studied nitrogenase is the iron-molybdenum dependent version of nitrogenase, which is the focus in this research. The MoFe protein and Fe protein also denoted as component I and component II respectively are the two proteins that comprise nitrogenase. The Fe protein is a 63 kDa homodimer that has a single Fe_4S_4 cluster at the dimer interface. The MoFe protein is a 240 kDa $\alpha_2\beta_2$-heterotetramer with two types of Fe-S clusters, the P-cluster and FeMo-co. The P-cluster, a Fe_8S_7 cluster, is at the interface of the α and β subunits of the MoFe protein, and FeMo-co is a Fe_7MoS_9C-(*R*)-homocitrate cluster (Figure 5) within the active site in the α-subunits. Each FeMo-co is conjugated at the terminal iron by a thiolate of a cysteine ($\alpha\text{-}275^{Cys}$) and at the other end on the molybdenum by the ε-N of a histidine ($\alpha\text{-}442^{His}$) (*60*, *61*) The-(*R*)-homocitrate is coordinated through its C-2 carboxyl and hydroxyl groups to the molybdenum (*62*). The Fe-

protein binds Mg-ATP, docks to the MoFe protein, hydrolyzes the bound Mg-ATP, and couples the liberated free energy to inter-protein transfer of a single electron to the P-cluster of the MoFe protein (Equation 1). Electrons are then transferred from the P-cluster to FeMo-co where an eight electron reduction of N_2 and protons occur producing NH_3 and H_2 (Equation 1)(*10*). In the absence of any substrates, such as dinitrogen or acetylene, FeMo-co readily reduces protons to form dihydrogen (*63, 64*)

$$N_2 + 8e^- + 16MgATP + 8H^+ \rightarrow 2NH_3 + H_2 + 16MgADP + 16P_i \quad \text{(Eq 1)}$$

Toward the goal of developing a novel advanced material for photocatalytic H_2 production, we have formed a complex between FeMo-co, one of Nature's best reductive catalysts, and CdSe, a proven photoreductive nanoparticle. A CdSe●FeMo-co system could be a passive way to produce dihydrogen as an alternative fuel source. Substantiation that a CdSe●FeMo-co could photocatalytically generate H_2 could be found with the precedence of CdSe nanoparticles being able to reduce methyl viologen (MV^{2+}) by photoactivation. The CdSe●MV^{2+} system was illuminated and caused reduction of the MV^{2+} where the reduced state was observed by transient absorption spectroscopy (*23*). The reduction potentials of MV^{2+} and FeMo-co are very close (-0.460 mV and -0.465 mV, respectively)(*40, 65*). Therefore, CdSe should be able to photo-reduce FeMo-co in the same way that it reduces MV^{2+}. With illumination of a CdSe●FeMo-co system, CdSe should photo-reduce FeMo-co and then FeMo-co should catalyze the reduction of dissolved protons to evolve dihydrogen (Figure 6).

This study describes how CdSe and FeMo-co were complexed with and without a protein, in organic and aqueous media, and were used for generation of dihydrogen. Because of the readily

available source of solar energy, the generation of dihydrogen through photo-catalysis represents a promising option to secure a sustainable energy source for the future.

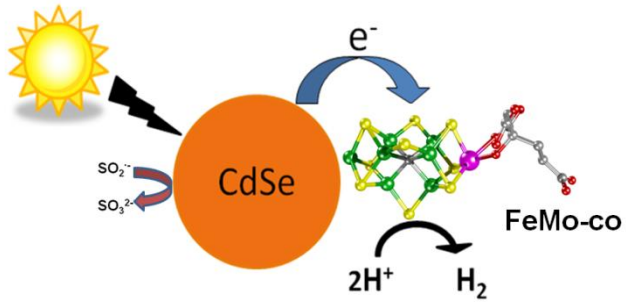

Figure 6. Representation of CdSe Nanoparticles Complexed with FeMo-co.
Visible light excites CdSe enabling photoreduction of FeMo-co that catalyzes the production of dihydrogen from available protons in solution.

Materials and Methods

All chemicals used were purchased from Fisher, Sigma and Aldrich.

UV-Vis Absorbance and Fluorescence Emission Spectroscopy.

UV-visible absorbance spectra were acquired on a Perkin-Elmer Lambda 750S spectrophotometer. Fluorescence emission was measured using a Horiba Jobin Yvon Fluoromax 4 Spectrofluorometer at excitation slit widths of 2 or 3 nm and emission slit widths of 2 or 3 nm.

Synthesis of CdSe-TOP nanoparticles.

CdSe-TOP quantum dots with particle sizes of 2.4 to 2.7 nm were synthesized using a high temperature pyrolysis method (*23*) The CdSe nanoparticles with the capping agent, trioctylphosphine (TOP), were solubilized in chloroform and prepared according to published methods (*24*, *25*). The nanoparticles were stored anaerobically in the dark at 4 °C. The quantum dots were characterized by UV-vis absorbance and fluorescence emission spectroscopy. The CdSe nanoparticle size was determined by noting the first absorption peak, using the published method relating absorbance to nanoparticle diameter. The calculated extinction coefficient based on the particle diameter was 59,598 $M^{-1}cm^{-1}$ that enabled the determination of CdSe nanoparticle concentration (*18*). Absorbance (λ_{max}), was 515 nm and fluorescence emission (Em_{max}), when excited at 410 nm was 531 nm (*66*). CdSe-TOP will be used to designate TOP capped CdSe that is soluble in organic solvents.

Purifications of MoFe Protein, NafY, and Extraction of FeMo-co.

MoFe protein was purified from *Azotobacter vinelandii* strain DJ995, expressed with a polyhistidine tag fused on the C terminus of nifD, as previously described (*67*). NifD is the α-subunit of MoFe protein (NifDK). MoFe protein purity was judged to be 95% pure using SDS-PAGE (*68*), stained with Coomassie blue. Quantification was performed by Biuret assay (*69*). FeMo-co was acid extracted into N-methylformamide (NMF) solution using previously published methods (*39*), and quantified by assaying Fe concentration as previously described (*70*). The degassed NMF solution was adjusted to a pH of 8.0 with triethylamine and sodium

dithionite was anaerobically added to a final concentration of 1 mM. To assess FeMo-co activity, FeMo-co was added to an *apo*- form of the MoFe protein to form the *holo*-MoFe protein and assayed by measuring hydrogen evolution activity (*71*)

NafY was expressed in *Escherichia coli* and purified according to previously published procedures (*56*). Protein purity was assessed by SDS-PAGE and quantification was performed by the bicinchoninic acid assay method using bovine serum albumin as a standard (*72*).

Assembly of Complexes between CdSe-TOP and FeMo-co.

All sample preparations were performed in anaerobic septum sealed cuvettes or vials, using standard Schlenk line techniques or performed in an anaerobic chamber with 5% (v/v) hydrogen/nitrogen and less than 1 ppm O_2. Gas tight syringes were used to perform liquid transfers for all experiments.

X-Band EPR Spectroscopy.

X-band EPR spectra were recorded on a Bruker Elexsys E580 X-band spectrometer equipped with a Bruker standard rectangular TE102 resonator and fitted with an Oxford Instruments ESR900 helium flow cryostat. Modulation frequency was set at 100 kHz and modulation amplitude was set at 1.00 mT (10.0 G). The microwave frequency was approximately 9.45 GHz with the exact frequency noted for each spectrum and used for calculation of *g* values. All spectra were recorded at 5 K using a microwave power of 2.0 mW. Each trace was a sum of five scans unless stated otherwise.

Assembly of CdSe-MSA●NafY-FeMo-co Complexes.

Water soluble CdSe nanoparticles were synthesized following a published procedure with some modifications. CdSe-TOP nanoparticles were synthesized by high temperature pyrolysis and dissolved in octadecene (*73*). Characterization was performed by UV-vis absorbance (λ_{max} - 515 nm), and fluorescence emission (Em_{max} -532 nm when excited at 410 nm). Size determination of the quantum dots was 2.4 nm diameter and the calculated extinction coefficient was 59,598 M^{-1} cm^{-1} (*66*) To exchange the surface capping agent from trioctylphosphine to the aqueously soluble mercaptosuccinate, a reaction in methanol was performed under reflux at pH of 10. Fourfold molar excess of the quaternary base, tetrabutylammonium hydroxide, as compared to the added moles of mercaptosuccinate was used to fully deprotonate the mercaptosuccinic acid. The use of a solution of the base dissolved in methanol (40% w/v) was essential to avoid introducing any unnecessary water into the system.

During the work-up steps, the water soluble quantum dots were precipitated on the inner surface of the round bottom flask using a rotary evaporator, instead of precipitation by centrifugation as described in the published procedure. The quantum dots inside the flask were dried under vacuum overnight and resolublilized in aqueous 25 mM Tris, pH 8.0, the following day. The mercaptosuccinate functionalized CdSe quantum dots dissolved in 25 Mm Tris solution had an extinction coefficient of 73,681 M^{-1} cm^{-1} (*66*) Their diameter was calculated to be 2.6 nm with λ_{max} at 525nm and an Em_{max} at 538 nm. CdSe-MSA will be used to designate the mercaptosuccinate capped water soluble quantum dots.

All samples with CdSe-MSA were set up in septum sealed cuvettes or vials using standard Schlenk line techniques or in an anaerobic chamber with 5% (v/v) hydrogen/nitrogen

with less than 1 ppm O_2. Gas tight syringes were used to perform liquid and gaseous transfers in all the experiments.

A reaction between CdSe-MSA and methyl viologen was performed with aqueous soluble CdSe-MSA (720 nM) combined with methyl viologen (1.47 mM) and dithiothreitol (14.7 mM), with adaptations to a published method (*74*). The samples were illuminated for 30 second intervals followed by UV-vis absorbance for a total time of eight minutes.

Preparation of the NafY●FeMo-co complex was performed using a modification of previously described procedures (*75*). NafY in 25 mM Tris and FeMo-co in NMF solution were combined with stepwise aliquots of the FeMo-co such that the NMF solution did not exceed 3% (v/v) NMF so as to avoid denaturing of the protein.

Photo-catalyzed dihydrogen production.

CdSe-MSA and NafY●FeMo-co were mixed together in 3.0 mL anaerobic crimped seal vials in a total reaction volume of 1.5 mL, 25 mM Tris at pH 8.0, 0.2 mM $Na_2S_2O_4$, 2μM to 16 μM CdSe-MSA nanoparticles and 2 μM NafY●FeMo-co.

The dithionite concentration was initially kept at 0.2 mM so as to allow the CdSe-MSA and NafY●FeMo-co to bind to each other with minimal interference from the dithionite. After one minute of mixing, the $Na_2S_2O_4$ concentration was increased to 2.0 mM. Prior to illumination, samples were thoroughly degassed and exchanged into argon by multiple rounds of vacuum and 3 psi of O_2 free argon. Reaction samples for the reduction of methyl viologen or dihydrogen production experiments were illuminated using a 500 Watt halogen lamp. Samples were kept 8

cm from the light source. The samples were continuously illuminated and the temperature was kept at 30 ± 2 °C. Illumination times are indicated in figure legends.

Assay for the evolution of dihydrogen was performed by sampling (250 μL) the headgas of reaction vials using a gas-tight syringe and analyzing on a Hewlett Packard Series II 5890 Gas Chromatograph equipped with a Restek 13X 60/80 molecular sieve column and a thermal conductivity detector. Argon flow was set at 5.0 mL/min. Hydrogen peaks were standardized using quantitative hydrogen standards prepared in crimped seal vials of the same size and same headgas volume as the samples with 1.5 mL water volume according to published procedures (*76*).

Results

Assembly of CdSe-TOP•FeMo-co complex.

The intent for forming a CdSe-TOP●FeMo-co complex was to take advantage of the CdSe-TOP's photocatalytic activity and FeMo-co's ability to catalyze H^+ reduction. For the two components to work together and utilize solar energy to facilitate electron transfer for dihydrogen production, the formation of a stable complex between CdSe-TOP and FeMo-co would be required.

CdSe-TOP nanoparticles are characteristically photoluminescent. Hence fluorescence emission may be used to interrogate interactions between CdSe-TOP and other chemical species (*15*). Complex formation with another species may result in static quenching of the CdSe-TOP fluorescence emission. Static quenching may be observed if the interaction between different

components allows for overlap of molecular orbitals (*77*). Quenching of the CdSe-TOP fluorescence emission was used to determine if the added FeMo-co was bound to the surface of the nanoparticle.

The CdSe-TOP•FeMo-co system has some advantages as compared to CdSe in aqueous solvents. CdSe-TOP nanoparticles in organic solvents have significantly greater photo-activity as compared to the same sized CdSe nanoparticles in aqueous media (40 times more photoluminescence). CdSe-TOP nanoparticles exhibit the photo-activity due to their intrinsic quantum confinement characteristic. The quantization effects are observed because their excitons, excited electrons and their electron holes are confined within small regions of space. Although quantum dots are comprised of approximately 100 binary units of CdSe in three dimensional space, they are still small enough to exhibit the quantum properties of a single CdSe unit (*78*). Quantum confinement also contributes to the observed property of nanoparticle color, i.e. the energy for excitation corresponding to the bandgap, which can be tuned by adjusting nanoparticle size within the parameters of its Bohr exciton radius (5.6 nm for CdSe) (*19*). The size of the CdSe-TOP nanoparticles was dictated and controlled by managing reaction conditions such as temperature and time during its synthesis.

Another advantage to the CdSe-TOP•FeMo-co system was the ability to use chloroform as a solvent and its miscibility with NMF solution, which is used to extract FeMo-co from the MoFe protein. In addition, the NMF solution contains 1 mM sodium dithionite. The sodium dithionite serves two purposes in the CdSe-TOP•FeMo-co system of being an oxygen scavenger and as a source of electrons (*71*). FeMo-co is very oxygen sensitive having an approximate half-life of about 30 seconds after air exposure (*71*), and the sodium dithionite prevents oxidative

degradation of FeMo-co. When light excites CdSe-TOP, an electron is excited to a higher energy state moving into the conduction band. This generates an electron hole in CdSe's valence band. The dithionite acts as a sacrificial donor to quench the electron hole (*20*).

As described earlier, fluorescence emission was used to probe the interaction between CdSe-TOP and FeMo-co. Incremental 1 μL additions of FeMo-co (60 μM stock) were made to a 10 μM solution of CdSe-TOP nanoparticles and the sample was inspected by both UV-vis absorbance and fluorescence emission spectroscopies after each addition. With the addition of either the FeMo-co or solvent NMF solution, the UV-vis absorbance (data not shown) did not change significantly, indicating that the integrity of the CdSe nanoparticles in solution was intact. In contrast, significant changes were observed in the fluorescence emission of CdSe-TOP. Progressive addition of FeMo-co to the CdSe-TOP solution resulted in the quenching of the CdSe-TOP fluorescence emission (Figure 7A and 7C).

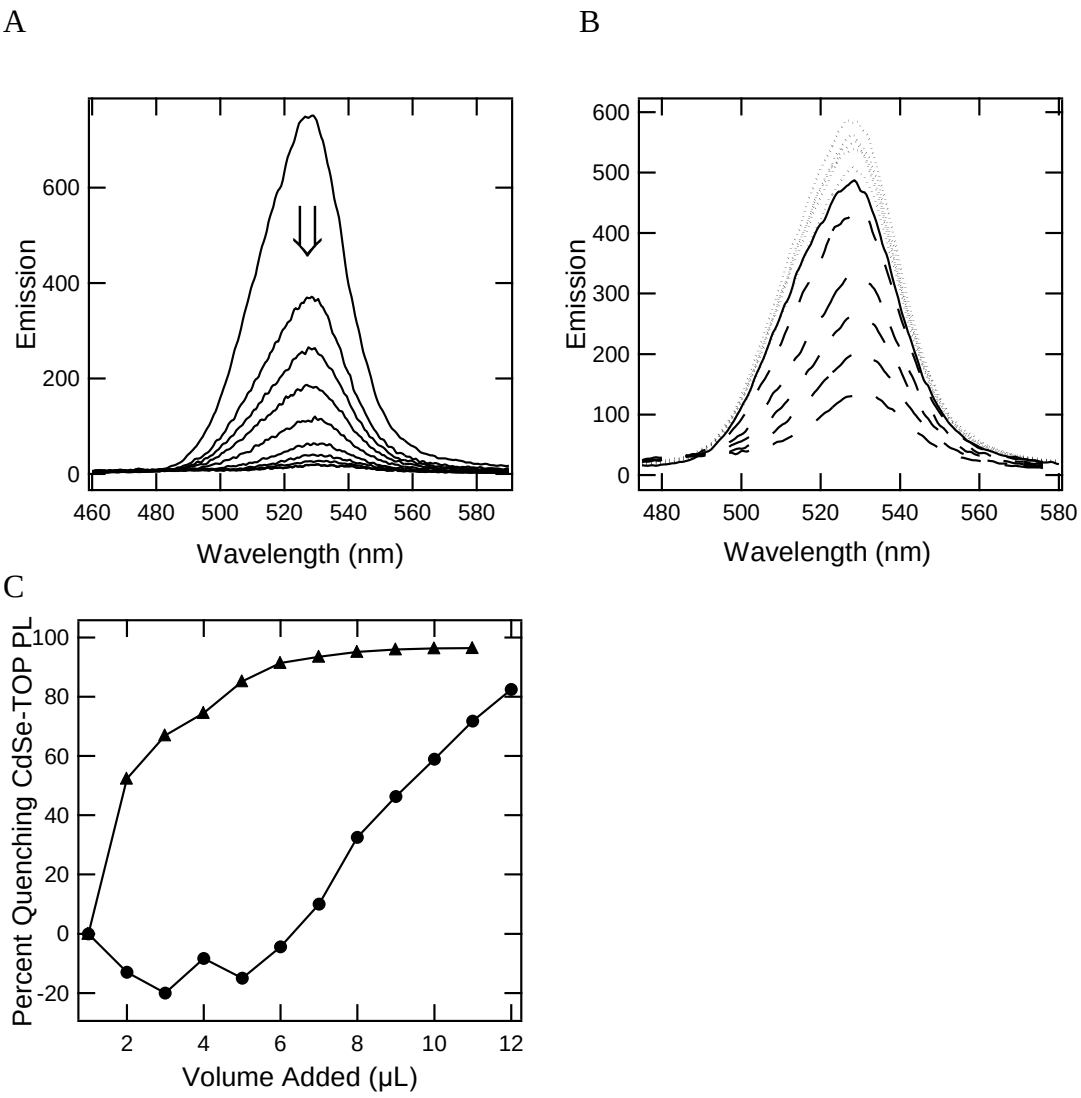

Figure 7. CdSe-TOP Fluorescence Quenching with Added FeMo-co or NMF.
(A) Fluorescence emission spectra of CdSe-TOP (10 μM) with sequential 1 μL additions of FeMo-co solution (60 μM stock). The plots show a decrease of fluorescence intensity for the CdSe-TOP. (B) Fluorescence spectra of CdSe-TOP with sequential additions of the same volumes of the solvent NMF solution as the FeMo-co additions. The solid black line is the CdSe-TOP before any additions. The first five additions of NMF are shown with dotted lines showing an increased photoluminescence. With the additions of 6-10 μL NMF, the CdSe-TOP fluorescence is progressively quenched. (C) The data in panels A and B are replotted as percent quenching to compare the quenching by FeMo-co (▲) and NMF (●).

A similar titration was performed using the solvent NMF solution used for the extraction of FeMo-co to serve as a control (Figure 7B and 7C). The addition of NMF to the CdSe-TOP solution enhances its fluorescence intensity with the addition of the first 5 μL. This effect to enhance the fluorescence has been reported before (*79*). The fluorescence intensity does decrease with the further addition, 6 to 10 μL, of the solvent NMF solution (Figure 7B.)

The degree of emission quenching with respect to the volume of either FeMo-co or NMF solution added (Figure 7C), clearly shows a difference between the additions of FeMo-co solution and the additions of NMF solution. The addition of only 5 μL of FeMo-co (60 μM in solution) was sufficient to quench 90% of the CdSe-TOP fluorescence emission. In comparison, only 10% of the fluorescence emission was quenched with the addition of an equivalent volume of the solvent NMF solution. Furthermore, quenching of the CdSe-TOP fluorescence by FeMo-co seems to saturate, somewhat suggesting a specific interaction. These data indicate that the CdSe-TOP nanoparticles and the FeMo-co do form a complex. Additionally, the CdSe-TOP quantum dots that were most efficient for forming a complex were in the size range of 2.4 to 2.7 nm diameter.

Despite the demonstrated fluorescence quenching of CdSe-TOP by the addition of FeMo-co, which suggests the formation of a complex, a question persisted whether the quenching is due to binding of FeMo-co that is structurally intact. To test this, air-oxidized FeMo-co was added to CdSe-TOP. If the FeMo-co had degraded during the formation of the complex, quenching of the CdSe-TOP fluorescence would not be likely.

Three samples of CdSe-TOP (10μM) were inspected by UV-vis absorbance and fluorescence emission before and after six μL additions of 1) 60 μM FeMo-co, 2) air exposed

degraded FeMo-co of the same concentration, or 3) solvent NMF solution. Addition of FeMo-co quenched 88% of fluorescence from CdSe-TOP (Figure 8 and Table 1), and addition of the solvent NMF solution caused 52% quenching, which represents a similar degree of fluorescence quenching in the titration experiments above. Significantly, the addition of degraded FeMo-co sample showed 61% of quenching, which is comparable to the extent of quenching observed with addition of the solvent NMF solution. Since the air exposed degraded FeMo-co was in NMF solution, the limited fluorescence quenching observed with the degraded $Fe^{2+/3+}$ was close to the fluorescence quenching observed with the addition of the same amount of NMF solution. Thus, structurally intact FeMo-co is binding to CdSe-TOP nanoparticles, causing CdSe-TOP fluorescence quenching. The flurorescence quenching observed is not due to potential dissolved $Fe^{2+/3+}$ in solution from degraded FeMo-co.

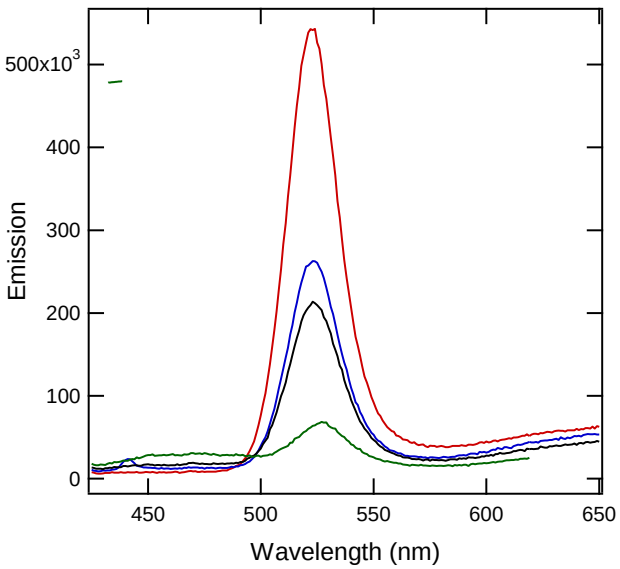

Figure 8. CdSe-TOP Fluorescence Quenching by FeMo-co.
The red trace is the control fluorescence emission spectrum of CdSe-TOP without any quencher. The blue trace is fluorescence emission spectrum of CdSe-TOP quenched by addition of the solvent NMF solution. The black line is the fluorescence emission spectrum with addition of air oxidized FeMo-co to CdSe-TOP. The green line is the emission spectrum of FeMo-co added to CdSe-TOP.

Table 1. Percent Quenching of CdSe-TOP Fluorescence by FeMo-co.

Additions to CdSe-TOP	Percent Quenching*
NMF,0.1 mM dithionite	51.7
Oxidized FeMo-co	60.7
Active FeMo-co (0.36 μM)	87.7

*CdSe-TOP fluorescence emission without additions is 518,000 arbitrary units. Percent quenching is a measurement of CdSe-TOP fluorescence after addition of reagents subtracted from fluorescence without the additions divided by fluorescence without additions times 100.

EPR Characterization of CdSe-TOP-FeMo-co Complex.

EPR spectroscopic analysis of Fe-S clusters allows for investigation of electronic structures, electronic spin states and configurations. Changes observed in characteristic signals can possibly indicate a different electronic spin state or configuration. Oxidation state changes can also be observed after electron transfers (*80*). FeMo-co has a characteristic $S = 3/2$ spin state signal in its dithionite reduced resting state and also an analogous signal in the dithionite reduced *holo*-enzyme (*81*). The CdSe-TOP nanoparticles show no EPR signal.

The fluorescence emission characterization of CdSe-TOP with added FeMo-co had suggested that CdSe-TOP•FeMo-co had formed a complex due to the quenching of fluorescence emission of the CdSe-TOP. With illumination of the CdSe-TOP, excited electrons could be transferred to the FeMo-co adsorbed on the CdSe-TOP surface with a potential observation of a change in the FeMo-co EPR signal due to an alteration in its electronic structure.

To achieve concentrations appropriate for EPR experiments (> 100 μM of EPR active species), a much higher concentration of the CdSe-TOP nanoparticles were required. To achieve such a concentration, CdSe-TOP was precipitated and then resuspended in a minimal volume of an alternative solvent. Tests for solubility of the precipitated CdSe-TOP nanoparticles were performed in three different solvents. In microcentrifuge tubes, 300 μL of 100 μM CdSe-TOP nanoparticles were precipitated with the addition of 1.0 mL of ethanol and then pelleted by centrifugation (5030 X g, for five minutes). The CdSe-TOP pellet was then resolubulized in 300 μL of three different solvents: NMF, acetone and ethyl acetate. The CdSe-TOP nanoparticles were soluble in the NMF and the ethyl acetate, but were insoluble in the acetone. NMF was

chosen to be the solvent for the EPR experiments since NMF is the best known solvent for stabilizing FeMo-co and it was observed to be miscible with chloroform.

To inspect if the CdSe-TOP•FeMo-co complex would stay intact during the ethanol precipitation and resolubilization to enable concentration of the sample, CdSe-TOP before and after mixing with FeMo-co were characterized by UV-vis absorbance and fluorescence emission. Concentrations of reagents were the same as used in the fluorescence emission experiments. Ethanol was added to the CdSe-TOP•FeMo-co sample and was centrifuged at 5030 X g for five minutes. The pellet was resolubilized in chloroform and the fluorescence emission spectrum showed no change from before the ethanol precipitation. The UV-vis spectra also showed no changes, and thus the CdSe-TOP●FeMo-co complex appeared to be intact after one ethanol wash.

Samples for EPR spectroscopy were prepared by mixing 3.0 mL CdSe-TOP (400 μM) with 0.67 mL FeMo-co (60 μM) and then precipitating with the addition of 10.0 mL of ethanol with rapid mixing on a vortexer. The sample was centrifuged (5030 X g, for five minutes) to pellet the precipitated CdSe-TOP•FeMo-co. The pellet was solublilized by adding 250 μL of solvent NMF solution and vortexed. The sample was injected into a sealed anaerobic 4 mm quartz EPR tube and frozen in liquid nitrogen.

The three control samples were as follows. The first control, CdSe-TOP, showed no EPR signal (not shown). The second control was that of 180 μM MoFe protein (2 FeMo-co clusters per protein molecule), (Figure 9, Trace 1). The third control was that of 60 μM FeMo-co (Figure 9, Trace 2), (*82*, *83*).

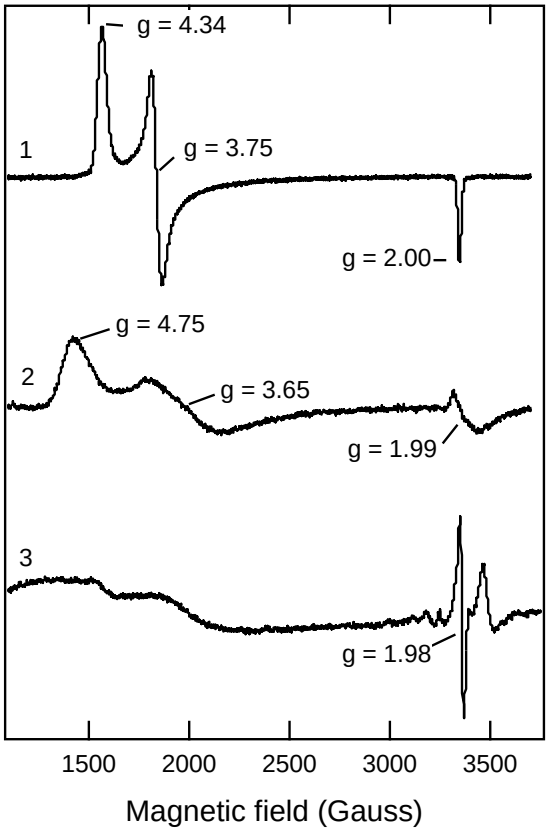

Figure 9. CdSe-TOP•FeMo-co System Investigated by EPR.
EPR spectra are shown for MoFe protein (180 μM) (trace 1), FeMo-co (60 μM) (trace 2) and CdSe-TOP•FeMo-co complex with CdSe-TOP (2.5 mM), FeMo-co (200μM), (trace 3). Inflection points for the EPR absorption peaks are indicated by *g*-values.

The EPR inspection of the CdSe-TOP•FeMo-co (Figure 9 Trace 3) shows significant changes compared to the MoFe protein or isolated FeMo-co. First, the EPR signal at g = 4.3, 3.7 and 2.0, representing the S = 3/2 spin state, is largely diminished and the S = 1/2 spin state sub manifold signal had a g value of 1.99. Second, a significant new signal at g = 1.98 and 1.97 is observed. Significantly, an EPR signal in this region of the spectra is from an S = 1/2 spin state and suggests a change in electronic spin state, possibly due to reduction of the S =3/2 state of FeMo-co. Similar S = 1/2 spin state signals have been observed with several trapped turnover

intermediates of MoFe proteins and MoFe protein variants (*84*). Such intermediates are associated with turnover states that are relevant to the mechanisms of substrate reduction for various substrates. Another $S = 1/2$ spin state signal has been observed in a trapped state during proton reduction by FeMo-co in a nitrogenase $\alpha\text{-}70^{Ile}$ MoFe protein variant (*85*). Thus, the $S = 1/2$ spin state in this experiment may be interpreted to indicate an electronic change in FeMo-co.

To further probe if the change in electronic spin state observed for the CdSe-TOP•FeMo-co may indeed be due to light catalyzed electron transfer from the CdSe, light dependent experiments were performed. FeMo-co should appear in the resting state with its $S = 3/2$ spin state signal if there would be no photo-initiated electron transfer from the CdSe-TOP. An additional sample was prepared as the CdSe-TOP•FeMo-co sample in the light; however, before being frozen in the EPR tube it was exposed to air. This sample would verify that the new $S = 1/2$ EPR signal was indeed a reduced state of FeMo-co and not $Fe^{2+/3+}$ ions in solution from degraded FeMo-co. Preparation of these samples in the dark were met with technical difficulties and EPR inspection of these samples yielded no interpretable data.

Assembly of CdSe-Mercaptosuccinic Acid•NafY•FeMo-co Complex.

CdSe-TOP quantum dots in organic solvents are well known for their photo-activity, but the presence of an organic solvent limits their use with most protein applications. Three approaches to achieve water soluble CdSe quantum dots have been reported (*86*). One is by a direct synthesis method which uses an arrested precipitation technique in aqueous media (*26*). A second synthetic method encapsulates the organically soluble quantum dot in a polymerized silica shell functionalized with polar groups or an amphiphilic polymer coating that can

significantly add to the quantum dot diameter (*27*). Third, a ligand exchange method replaces the capping agent on the nanoparticle from trioctylphosphine or trioctylphosphine oxide with a mercapto-carboxylic acid (*28*).

A disadvantage with water soluble nanoparticles is their tendency to be less photo-active than their organic counterparts. If there is a lack of coordinated surface atoms, then there will be trapped states on the surface of the quantum dot that lie within the band gap. When light illuminates the nanoparticle and excites electrons to the conduction band, there will be more alternative pathways available for relaxation back to the ground state via the trapped states (*28*). Thus the desired energy or electron transfer to any adsorbed surface species may not occur. The challenge was to determine the best consistent method to achieve the most photo-active aqueous soluble quantum dots.

Methods to produce the most luminescent quantum dot were explored through two efforts to directly synthesize the quantum dots (*29, 87*), and by three methods to exchange the capping agent (*73, 88, 89*). Capping agents affect the photoluminescent properties of the nanoparticles. The most luminescent quantum dots with a target diameter (2.4 to 2.6 nm) were produced by a published method with some modifications using mercaptosuccinic acid (MSA), as the capping agent (*73*). The mercaptosuccinic acid was suggested to be the best capping agent to enhance photoluminescence (*29*). The previous complex between CdSe-TOP and FeMo-co took advantage of both reactants being in organic solvents. When isolated FeMo-co is mixed in water, even though kept anaerobic, the FeMo-co quickly hydrolyzes. For FeMo-co to combine with aqueous CdSe and remain intact, complexation to proteins was required.

NafY is a low molecular weight protein that binds FeMo-co with high affinity (K_d of 62 nM) (*56*). Combining FeMo-co with NafY and conjugating this species to CdSe-MSA may be a useful way to place the FeMo-co in close proximity to the photo-reducing CdSe-MSA. The NafY●FeMo-co conjugated to CdSe in a Tris buffered system would be a means for isolated FeMo-co bound to NafY to be in an aqueous system. The 26 kDa NafY●FeMo-co system (*90*) has a further advantage, compared to the 250 kDa MoFe protein that contains FeMo-co in a more buried configuration, of being smaller and better accessibility to FeMo-co (*14*). Furthermore, the aqueous solvent would be a better proton source for dihydrogen evolution.

Although aqueous CdSe quantum dots are less luminescent (by a factor of 40), than CdSe in an organic solvent of the same diameter, thus indicating a lower quantum yield, their ability to be involved in electron transfer was anticipated. Inspection of the CdSe-MSA nanoparticles was performed to determine their capability to form complexes and their photoactive capability to transfer electrons to FeMo-co and thereby perform interesting and useful chemistry.

To use CdSe-MSA in experiments with a FeMo-co species, demonstration of CdSe-MSA forming a complex with proteins was necessary. CdSe-MSA was added in incremental amounts to bovine serum albumin (BSA) according to a published method and thereby demonstrated conjugation between the two reagents (*91*). The published procedure had used CdSe capped with mercaptoacetic acid instead of mercaptosuccinic acid. The samples were excited at 280 and 410 nm in a fluorescence emission investigation. Control samples of BSA alone and CdSe-MSA alone were excited at both wavelengths with no observable changes seen in the samples.

Emission at 347 nm was from the BSA and emission from the 532 nm was attributed to the CdSe-MSA. The BSA fluorescence emission was quenched 78% with the addition of 300 μL of CdSe-MSA. The ratio of the two components, BSA:CdSe-MSA, was 1:3.5 . The conclusion was that CdSe-MSA and BSA protein had formed a complex.

To probe complex formation between CdSe-MSA and NafY protein, the two were combined by adding incremental amounts of CdSe (14.6 μM stock) to NafY (500 nM) (Figures 10A and 10B). The sample was excited at 280 nm to observe tryptophan emission at 347 nm. The sample was also excited at 410 nm to verify that the observed peak at 532 nm could be attributed to the CdSe-MSA being added in increasing amounts. Eighty percent of the NafY fluorescence quenching was observed with 30 μL addition of CdSe-MSA, which is a 1:1 ratio between NafY●CdSe-MSA (Figure 10B). A NafY control sample and a CdSe-MSA control sample showed no changes when excited at 280 nm and 410 nm. Figure 10C shows the data from 10A replotted as percent quenching of NafY fluorescence versus concentration of CdSe-MSA. Figure 10D shows the data from 10B replotted as CdSe-MSA fluorescence emission versus concentration of CdSe-MSA.

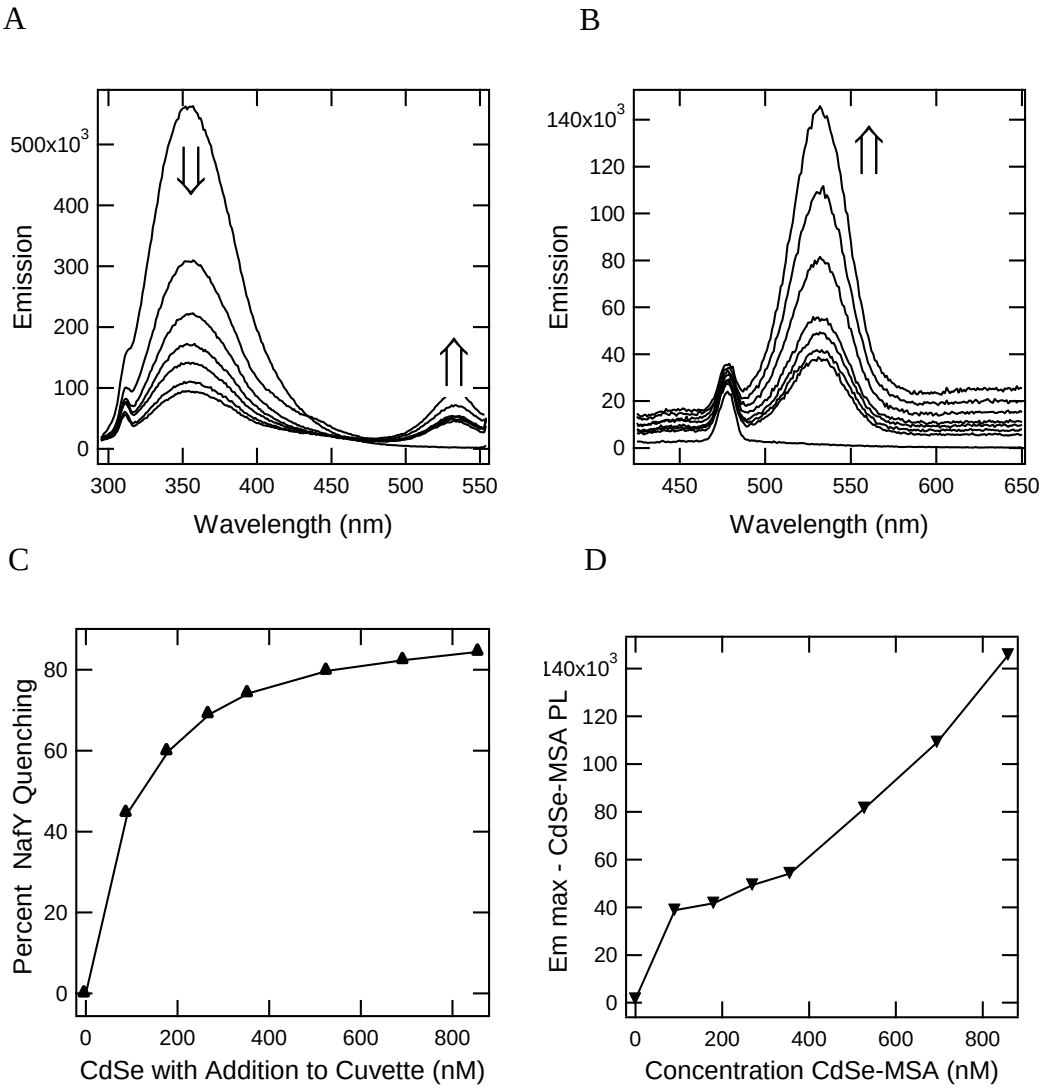

Figure 10. NafY Protein and CdSe-MSA Complex Formation Investigated by Fluorescence Quenching.

(A) NafY protein excited at 280 nm showing progressive fluorescence quenching at 347 nm with additions of CdSe-MSA seen. There is also an emission at 532 nm that increases as more CdSe-MSA is added. (B) Excitation of the same sample at 410 nm. With this emission the second emission in panel A is confirmed to be from the CdSe-MSA. (C) Replot of the data in A shows percent NafY quenching versus CdSe-MSA concentration. The plot shows a saturation type curve indicating the formation of a complex. (D) Replot of the data in B shows increasing photoluminescent intensity with increasing CdSe-MSA concentration.

Additionally, Forster resonance energy transfer (FRET), could be interpreted from the fluorescence emission experiments. Two sets of emissions (347 nm and 532 nm) were observed (Figure 11). Emission at 347 nm is from excitation of the tryptophans in NafY protein that acts as a donor for CdSe-MSA, which emits at 532 nm. The first emission at 347 nm (rust brown trace) shows NafY before addition of CdSe-MSA. The second emission (forest green trace) exhibits quenching of NafY fluorescence along with an acceptor emission at 532 nm from CdSe-MSA demonstrating FRET. When the sample was excited at 410 nm, the emission at 532 overlapped the emission observed with excitation at 280 nm confirming that the 532 nm emission was indeed from CdSe-MSA. FRET emission can only be observed when two species are close in proximity hence the conclusion was that NafY and CdSe-MSA had formed a complex.

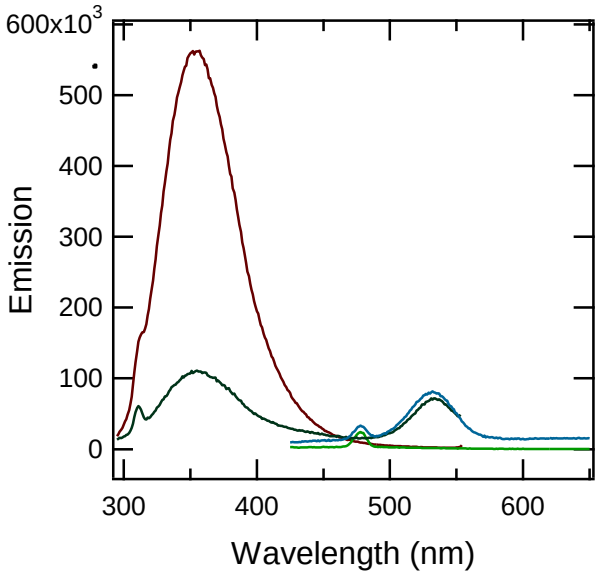

Figure 11. FRET Emission in NafY-CdSe-MSA Complexed System Shown in Replots of Data from Figures 5A and 5B.
Excitation of the NafY samples was at 280 nm. The emissions at 347 nm are NaY before (rust brown) and after (forest green) addition of 30 μL CdSe-MSA. The emission at 347 serves as the donor for the CdSe-MSA. The forest green peak shows a second emission that is the acceptor demonstrating FRET emission. The blue peak is the same sample with the addition of the CdSe-MSA excited at 410 nm and emitting at 532 nm. The pale green is NafY before the addition of CdSe-MSA excited at 410 nm.

To address the issue of lesser photo-activity of the water soluble quantum dots as compared to the organically solvated nanoparticles, an experiment with aqueous CdSe-MSA nanoparticles was performed. The hypothesis was that despite the photo-activity being less, the water soluble CdSe-MSA quantum dots would be able to perform a photo-induced electron transfer to a complexed species adsorbed onto their surface. To test the photocatalytic reduction activity, methyl viologen was combined with and CdSe-MSA. Dithiothreitol (DTT) would be used as a sacrificial electron donor to refill electron holes generated after electrons were excited to the conduction band from the valence band in CdSe-MSA. Reduction of the methyl viologen, MV^{2+}, was monitored by increasing absorbance peaks at 395 nm and at 603 nm with increasing times of illumination.

CdSe-MSA (720 nM), methyl viologen (1.47 mM) and dithiothreitol (14.7 mM), were combined and monitored by UV-vis absorbance. The sample was illuminated for 30 seconds and followed by UV-vis absorbance. This process was repeated for a total of eight minutes. To further test the photocatalytic ability of the system, the sample was first exposed to air to oxidize the reduced methyl viologen. Next, the cuvette was resealed and put on the manifold to make the headspace anaerobic by replacing it with argon. The photo-induced reduction experiment was repeated. Another air oxidation was followed by a third repetition of the experimental procedure. The first control sample was a solution of methyl viologen and dithiothreitol which underwent the same illumination times and UV-vis absorbance characterization. The second control was the CdSe-MSA for which the same experimental procedure was followed. A third sample was set up with the three reactants and kept in the dark for 16 hours.

The results show increasing absorbance at both 395 nm and at 603 nm with increasing periods of illumination (Figure 12A). The data for the absorbances at 603 nm were replotted as absorbance intensity versus time of illumination (Figure 12B). After exposing the sample to air and repeating the illumination and UV-vis absorbance measurements, the sample again demonstrated increasing absorbances at 395 and 603 nm with increasing periods of illumination. Interestingly, the CdSe-MSA-methyl viologen solution turned progressively more intense in blue color with increasing periods of illumination, indicative of absorption at 603 nm. When the sample was exposed to air, it lost the blue color and was orange from the CdSe. When the second round of illumination progressed the blue color returned to the sample. When the third repetition was performed, the same results were observed. The three controls showed no increasing absorbances at 395 nm or 603 nm with illumination. Additionally a concentration dependent experiment was performed with twice the CdSe-MSA (1.4 mM). The results showed that the absorbance peak at 603 nm increased more rapidly with the higher concentration of CdSe-MSA and thus showed a general trend of concentration dependence in the photo-reduction of methyl viologen (Figure 12B). The conclusion was that the CdSe-MSA quantum dots were photoactive and able to perform photo-reduction of adsorbed species, MV^{2+} in this case**,** when illuminated with intense visible light.

A B

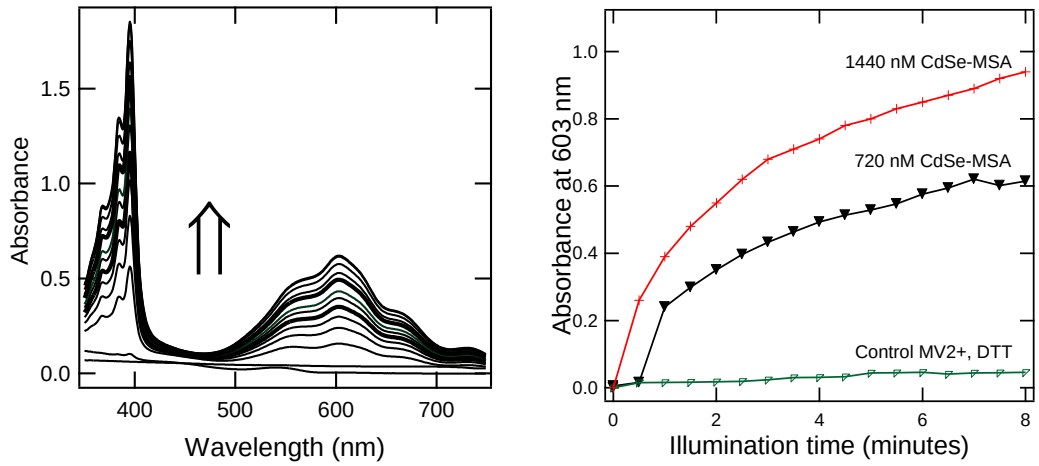

Figure 12. Photo-activated Time Dependent Reduction of MV^{2+} by Excited CdSe-MSA. (A) Absorbance spectra showing time dependent light induced reduction of methyl viologen by CdSe-MSA (0.72 μM). Methyl viologen (1.47 mM) and dithiothreitol (14.7 mM) were added prior to illumination, (B) Replot of data in A shows time dependence increase in reduced methyl viologen absorption at 603 nm (720 nM CdSe-MSA) (black trace) compared to the control sample (green trace). Additionally a concentration dependent absorption of twice the amount of CdSe-MSA is shown (1440 nM) (red trace).

EPR Characterization of CdSe-MSA•NafY●FeMo-co.

Experiments above present evidence that the CdSe-MSA will complex with the NafY protein and that CdSe-MSA is able to photo-reduce a species adsorbed onto its surface. Thus, NafY●FeMo-co being close in proximity to CdSe-MSA should allow photo catalyzed reduction and possible post-illumination changes in the electronic structure of FeMo-co that could be observed by EPR spectroscopy.

NafY●FeMo-co samples were prepared prior to forming a complex with the CdSe-MSA. NafY protein was diluted to approximately 1.0 μM in 25 mM Tris, pH 8.0, 0.5 mM sodium dithionite in a stirred ultrafiltration cell fitted with a YM10 membrane (Millipore). To prevent

precipitation of NafY, additions of FeMo-co to the stirred cell ultrafiltration device containing NafY were made such that the NMF, solvating FeMo-co, did not exceed 3% (v/v). Repeated concentration and dilution steps were performed with each addition of FeMo-co. After the last addition of FeMo-co, 1.5 mL of degassed CdSe-MSA (30 μM) with 0.4 mM sodium dithionite was added. The solution was concentrated further to minimize the volume and then transferred to a 30,000 MWCO Centricon (Millipore) and kept anaerobic in JA-20 centrifuge tubes. Centrifugation was performed at a centrifugal force of 5000 X g to reach the desired concentration. The sample was then injected into 4 mm EPR quartz tubes and frozen in liquid nitrogen. The final concentration of the sample was 400 μM CdSe-MSA, 200 μM NafY●FeMo-co.

Control samples were as follows. The first was a FeMo-co sample used to comprise the CdSe-MSA●NafY●FeMo-co samples. The second control was a NafY●FeMo-co sample. The third was a CdSe-MSA●NafY●FeMo-co sample prepared in the dark. There should have been no change observed in the $S = 3/2$ spin state signal of FeMo-co for the sample of CdSe-MSA●NafY●FeMo-co prepared in the dark. The fourth control was the CdSe-MSA●NafY●FeMo-co sample prepared as previously described under strict anaerobic conditions throughout, but before being frozen it was exposed to air. With air exposure, FeMo-co should oxidatively degrade, resulting in ferrous and/or ferric ions in solution. This control sample would demonstrate that any change seen with the FeMo-co signal, did not arise from dissolved iron in solution. One last control sample was that of CdSe-MSA alone at a concentration of 400 μM.

The FeMo-co control spectrum showed an EPR signal ($g = 4.65$, 3.44 and 1.97) for an $S = 3/2$ spin state, characteristic of its dithionite reduced state when extracted into solvent NMF solution (Figure 13, Trace 1) (*83*). Compared to the MoFe protein, with FeMo-co in the active

site, the EPR spectrum for extracted FeMo-co was of a similar line shape, only broader. There were also comparable principal *g*-values, indicating that the general electronic structure was coincident. Binding of FeMo-co to NafY as in the NafY●FeMo-co yields a similar spectrum with g = 4.41, 3.71 and 2.07 (Figure 13, Trace 2), indicative of an S = 3/2 spin state (*56*). The binding of NafY does sharpen the line shape and is consistent with an additional ligand to FeMo-co, indicating covalent bonding between NafY and FeMo-co.

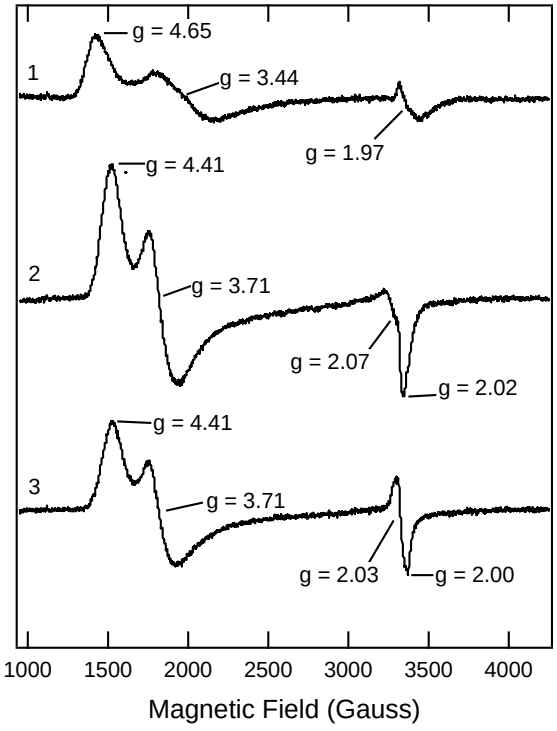

Figure 13. CdSe-MSA and NafY●FeMo-co Complex Formation Investigated by EPR. EPR spectra are shown for 60 μM FeMo-co (trace 1); 200 μM NafY●FeMo-co (trace 2); and CdSe-MSA●NafY●FeMo-co (trace 3) with little change from the spectrum in Trace 2. CdSe-MSA (400 μM), NafY●FeMo-co (200 μM).

EPR characterization of the CdSe-MSA●NafY●FeMo-co sample (Figure 13, Trace 3) showed an EPR signal for the $S = 3/2$ spin state, very similar to that of NafY●FeMo-co, significantly indicating that the electronic structure of FeMo-co bound to NafY was not being perturbed when the protein was interacting with the CdSe. There was a change in the $g \sim 2$ portion of the signal, corresponding to the $S = 1/2$ submanifold, but the rest of the signal ($g = 4.41$ and 3.71) remained unchanged. Hence, the structural integrity of FeMo-co, both molecular and electronic, should not be affected in this complex. This meant that FeMo-co survived the process and procedure for formation of the CdSe-MSA●FeMo-co ternary complex and would be suitable for photo-reduction.

The effect of light on the CdSe-MSA●NafY●FeMo-co sample was examined. The sample was sealed and thawed to room temperature anaerobically. The sample was exposed to a high intensity light for ten seconds. The sample was then immediately frozen in a hexanes-liquid nitrogen slush bath and re-characterized by EPR. The EPR spectrum (Figure 14, Trace 2), showed significant change as compared to this same sample's previous EPR spectrum (Figure 14, Trace 1, duplicate of Figure 13, Trace 3). The post illuminated sample shows a largely diminished EPR intensity for a species with the same line shape as the $S = 3/2$ state prior to illumination. The diminishment in signal intensity corresponds to a change in the population of $S = 3/2$ spin state to some other EPR silent state, suggesting that illumination initiated an electron transfer from CdSe-MSA to the adsorbed NafY●FeMo-co and therefore reducing it. This illuminated sample was then rethawed again, allowed to air oxidize, and refrozen. EPR inspection of the sample after air exposure (Figure 14, Trace 3), shows a sharp signal at $g = 2.0$, clearly from ferric irons. Thus, the conclusion was that upon exposure to intense light, the

electronic state of FeMo-co changed due to a possible electron transfer from the CdSe-MSA to the NafY●FeMo-co.

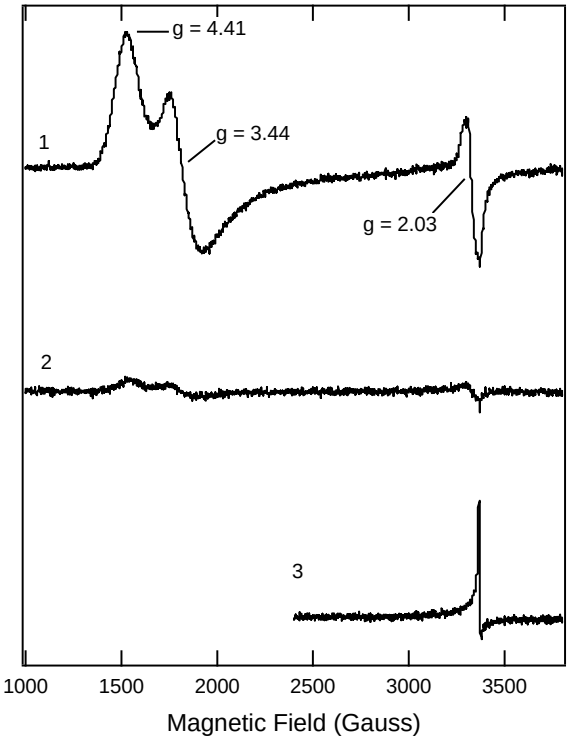

Figure 14. Illumination of CdSe-MSA●NafY●FeMo-co Complex Characterized by EPR. EPR spectra are shown for CdSe-MSA●NafY●FeMo-co (trace 1), after illumination with a mercury lamp (trace 2) and after air exposure (trace 3)

Photocatalyzed Dihydrogen Generation Experiments.

The experiments presented above demonstrate that the CdSe-MSA would form a complex with the NafY protein. The EPR based characterization of the CdSe-MSA●NafY●FeMo-co system showed that photo-reduction of FeMo-co upon illumination was likely. The CdSe-MSA had exhibited photo-reductive activity by its ability to reduce methyl viologen when illuminated with a 500 watt halogen lamp, detected by changes in UV-vis

absorbance. All of these evidences supported the hypothesis that a CdSe-MSA●NafY●FeMo-co system when illuminated should perform a reduction of aqueous protons as schematically described in Figure 15. Sodium dithionite (2 mM) would be added to the system for the dual purpose of 1) acting as a sacrificial electron donor to refill the electron hole after the generation of excitons in the CdSe upon illumination, and 2) acting as an oxygen scavenger to preserve the anaerobic environment for FeMo-co.

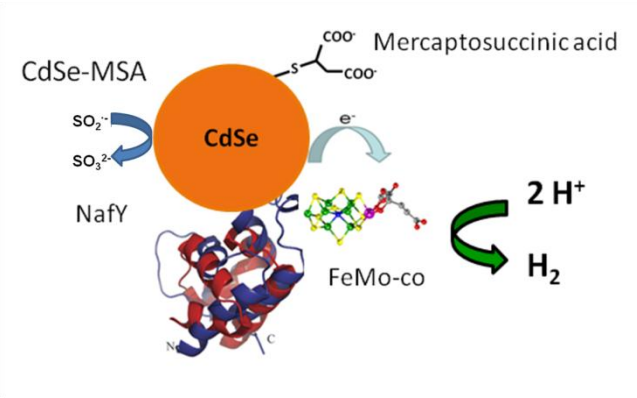

Figure 15. Representation of a CdSe-MSA●NafY●FeMo-co System Illuminated with Visible Light.
NafY●FeMo-co adsorbed on the surface of CdSe-MSA is photo-reduced and catalyzes the production of dihydrogen from protons dissolved in solution.

The dihydrogen generation experiments were performed with the variable being the extent of excess of CdSe-MSA with respect to NafY●FeMo-co, ranging in ratios of 8:1, 4:1, 2:1, 1:1 and 0.5:1. The NafY●FeMo-co was prepared as previously described with all the NafY bound with FeMo-co in a 1 to 1 ratio. The CdSe-MSA and NafY●FeMo-co were initially mixed with a low concentration of sodium dithionite (0.2 mM) and allowed to mix for one minute to form a complex without interference from sodium dithionite. After the initial time for complex

formation, additional sodium dithionite was added to a final concentration of 2.0 mM. All samples and controls were then positioned in front of the halogen lamp.

The head space gas of experimental and control samples were analyzed at multiple time points by gas chromatography. Samples from control reactions of CdSe-MSA, NafY●FeMo-co and CdSe-MSA●FeMo-co showed no signs of dihydrogen throughout. Interestingly, no dihydrogen was initially detected, but dihydrogen was detected after 24 hours of illumination from the reaction with 1 to 1 ratio of CdSe-MSA●NafY●FeMo-co. The other comparable reactions with other ratios of CdSe-MSA●NafY●FeMo-co showed no signs of dihydrogen generation. The experiment was repeated and still only the 1 to 1 samples showed dihydrogen production. All total there were four different repetitions of the reaction with 1:1 CdSe-MSA●NafY●FeMo-co that generated dihydrogen starting at 24 to 30 hours and continuing to produce dihydrogen until 114 hours (Figure 16A).

Two of the 1:1 samples were duplicates with samples analyzed at the same time and the data are shown in Figure 16B with error bars to demonstrate reasonable consistency. The generation of dihydrogen continued to between 100 to 114 hours when it appeared to stop. The maximum amount detected at that point was 316 nmols of dihydrogen produced over a period of 64 hours. With respect to the amount of FeMo-co used in the reaction, 105 nmol H_2 was produced per nanomole of FeMo-co. Stated as a specific rate, 1.8 nmol H_2/nmol FeMo-co/hour was the rate of dihydrogen production.

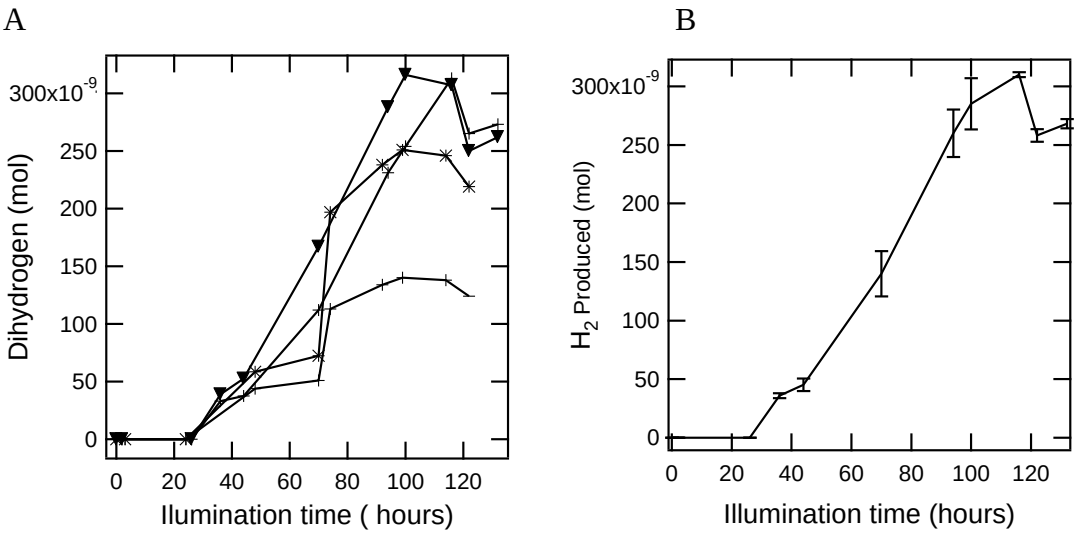

Figure 16. Time Dependent H_2 Production by a 1:1 CdSe-MSA●NaY●FeMo-co System. (A) Dihydrogen production by a 1:1 CdSe-MSA●NafY●FeMo-co system with illumination over130 hours in four different experimental sets with the same reaction conditions. (B) Two duplicate samples from within (A) with error bars.

The dihydrogen generation experiments were also attempted with MoFe protein in 100 mM MOPS, 1 mM dithionite, pH of 7.0 with added CdSs-MSA. Previously, a report (*14*) has shown the evolution of dihydrogen from MoFe protein with $Ru(bypy)_2$ attached.

As in the experiment above with the CdSe-MSA●NafY●FeMo-co, reactions with CdSe-MSA and the MoFe protein in varying ratios were set up. Control samples were CdSe-MSA (720 nM) and MoFe protein (360 nM). Head gas samples (100 μL) were analyzed by gas chromatography.

Initially, precipitation was observed with the higher ratios of CdSe-MSA to MoFe protein within the first 30 minutes of illumination. The 2 to 1 sample remained soluble and translucent for three hours but became cloudy thereafter. Solubility experiments were performed with

different pH buffered solutions of 7.0 to 8.0. The conditions with pH of 7.8 and 8.0 showed better solubility with the CdSe-MSA●MoFe protein system as compared to the lower pH values. No notable dihydrogen production was observed with these set of samples.

An additional reaction was performed with CdSe-TOP and FeMo-co. Given the high photo-activity of the CdSe-TOP, a sample in chloroform was combined with FeMo-co dissolved in NMF solution with all solutions and samples thoroughly degassed. The reaction was performed in a quartz cuvette with 5.0μM CdSe-TOP and 1.25 μM FeMo-co. The headspace was analyzed after one hour of illumination and determined to contain 28 nmol of dihydrogen. This reaction was performed lacking controls and needs to be re-performed in a proper experimental context with appropriate controls and variables. Although this result needs to be further investigated, the result is noteworthy due to its relative high activity. This system should be investigated further with duplicates, concentration dependencies and control samples to corroborate this result.

Discussion

Toward the goal of producing dihydrogen passively as an alternative fuel, a novel advanced material has been developed. CdSe nanoparticles complexed with FeMo-co, in both aqueous and organic solvent systems were illuminated with visible light and evolved dihydrogen. The CdSe-MSA●NafY●FeMo-co system when illuminated evolved dihydrogen consistently in four different experimental sets under the same reaction conditions. The CdSe-TOP●FeMo-co system produced dihydrogen in one sample, but awaits optimization. The rationale behind the experiments was as follows. CdSe nanoparticles with bandgap energy of 1.7 eV are able to

absorb incident light in the visible range, and create an electron-hole pair. CdSe nanoparticles were selected because their band gap energy is a close match to the thermodynamic potential of the H^+/H_2 couple. With the addition of NafY•FeMo-co to the CdSe nanoparticles, a complex was formed and thus put the NafY•FeMo-co in close enough proximity so that the exciton participates in electron transfer to the NafY•FeMo-co. This photo-induced reduction of FeMo-co then in turn catalyzed the reduction of protons in the aqueous solution to form dihydrogen.

Efficacy of Dihydrogen Generation from CdSe•FeMo-co Systems

There were some important discoveries along the way that contributed to the success of assembling a complex that when exposed to high intensity light would result in dihydrogen evolution. Utilization of CdSe-TOP and the CdSe-MSA nanoparticles with sizes that matched the bandgap energy associated with the thermodynamic potential of the H^+/H_2 couple and the adsorbed FeMo-co's reduction potential to facilitate its photo-reduction was crucial. CdSe nanoparticle sizes in the range of 2.4 to 2.7 nm in diameter appeared to be suitable for complex formation, monitored by fluorescence emission quenching and EPR. Particles of this size also were suitable for dihydrogen experiments.

Electron transfer between the excited CdSe nanoparticles and the adsorbed FeMo-co species was necessary to reduce FeMo-co. For this to occur, a complex had to form between CdSe and FeMo-co. This was demonstrated both in the organic CdSe-TOP•FeMo-co system and the aqueous CdSe-MSA•NafY•FeMo-co system by fluorescence emission quenching. To obtain evidence that in both complexed systems FeMo-co would be photo-reduced, samples were

interrogated by EPR spectroscopy. The EPR spectrum with the CdSe-TOP•FeMo-co system indicated that the population of the resting state $S = 3/2$ spin state was largely diminished. A new signal was observed at $g = 1.98$ and 1.97. This observed $S = 1/2$ spin state suggested a change in electronic spin state, possibly due to reduction of the $S = 3/2$ spin state of FeMo-co.

The EPR spectra of the CdSe-MSA•NafY•FeMo-co system showed a similar $S = 3/2$ spin state with a sharpened line shape consistent with an additional ligand (NafY) on FeMo-co. The complexed system spectrum was similar to the NafY•FeMo-co control sample indicating that the interaction between CdSe-TOP and FeMo-co had not perturbed the FeMo-co electronic structure. FeMo-co had survived the complex formation process and would be suitable for photo-reduction.

When the effect of light on this same CdSe-MSA•NafY•FeMo-co sample was examined, the EPR spectrum showed a significant change in the $S = 3/2$ spin state of FeMo-co compared to the previous EPR spectrum. The post illuminated sample showed a largely diminished EPR species with the same line shape as the $S = 3/2$ spin state prior to illumination. The diminished signal intensity corresponds to a change in the population of the $S = 3/2$ spin state suggesting that illumination had initiated an electron transfer from CdSe-MSA to the adsorbed NafY•FeMo-co.

The most successful system of the aqueous and organic systems with repeatable results for dihydrogen generation was a one to one CdSe-MSA•NafY•FeMo-co system. The maximum dihydrogen production was 316 nanomoles or 105 nanomoles H_2/nanomoles NafY•FeMo-co. There was one CdSe-TOP•FeMo-co sample which was illuminated and produced 28 nanomoles of dihydrogen in one hour; 22.4 nanomoles H_2/nanomoles FeMo-co. The experiment with the

CdSe-TOP•FeMo-co sample needs to be re-performed in a proper experimental context with appropriate controls and variables.

There were other considerations that are beneficial for analyzing the project. The interaction between the CdSe nanoparticles and the FeMo-co was different in the organic versus aqueous systems. The CdSe-TOP and the FeMo-co formed a complex in a direct interaction between the two. This resulted in an EPR signal at g = 1.99 resulting in an S = 1/2 spin state sub-manifold signal. Coordination of Fe in FeMo-co to the selenium of the nanoparticle may have produced this change in electronic structure of the FeMo-co (*80*).

In the aqueous system, the CdSe-MSA forms a complex with the NafY protein. Because of the size of NafY being approximately 15 nanometers and the FeMo-co bound to the NafY being 8 to 10 angstroms, this resulted in FeMo-co being close enough for electron transfer without being directly complexed with the nanoparticle. This was shown in the EPR spectrum of the CdSe-MSA•NafY•FeMo-co system when first combined. There was little change in the EPR signal at g = (4.41, 3.71 and 2.03) representing the S = 3/2 spin state; however, when this sample was illuminated with intense visible light, the EPR signal intensity was largely diminished indicating a change in the population of S = 3/2 spin states to some corresponding EPR silent state. An EPR silent signal is indicative of a diminished concentration of unpaired spins (*92*). This change was interpreted to mean that electron transfer had occurred between the excited CdSe-MSA to the FeMo-co inside NafY.

A few other factors to consider in the analysis of what led to the dihydrogen evolution are as follows. There is a distinct advantage of the aqueous based CdSe-MSA•NafY•FeMo-co system because of the ready source of protons as opposed to the chloroform dissolved CdSe-

TOP•FeMo-co. The samples were set 8 centimeters from the 500 watt halogen lamp, which promoted catalysis. Temperature maintenance was important in order to prevent degradation of the NafY protein conjugated to FeMo-co, 30 ± 2 °C. FeMo-co itself is not as temperature sensitive as the protein.

Possible Explanation for the Observed Hysteresis (Lag) of the CdSe-MSA•NafY•FeMo-co System for Dihydrogen Generation.

One observed phenomenon in the dihydrogen generation experiments using the CdSe-MSA•NafY•FeMo-co system is peculiar. The system did not show detectable dihydrogen until ~ 24 hours after the initiation of illumination. The most plausible explanation for the observed hysteresis (lag) could be that there were pH effects from dithionite reacting with water according to equations 1 and 2 (*93*). Over time the pH would decrease and more protons would be available for reduction. The sodium dithionite is in excess in the reaction vessel. Perhaps when it is depleted then the dihyrogen production levels off because protons are less available. An experiment interrogating the effects of pH on dihydrogen production either by direct changes in the pH of the buffered solution and/or changes in sodium dithionite concentration would be beneficial towards probing this issue.

$$S_2O_4^{2-} \rightleftharpoons 2\ SO_2^{\cdot -} \quad \text{(Eq. 1)}$$

$$SO_2^{\cdot -} + H_2O \rightleftharpoons H_2SO_3^{-} + H^{+} + e^{-} \quad \text{(Eq 2)}$$

Another possible explanation pertains to the way CdSe and FeMo-co interact. As light bombards the CdSe, electron-hole pairs are continually generated. The external and internal

generation of excitons, may alter the morphology of the CdSe nanoparticle. This may enhance the accessibility of the CdSe and the adsorbed species, thus resulting in more electron transfer events. This explanation has a flaw because the fluorescence emission quenching was immediately observed after the two reagents were mixed. If this alteration in morphology was necessary for adequate interaction, then a delay in the fluorescence emission quenching would have been observed. To interrogate this suggestion, more intense light could be used with the same experimental conditions, which should result in dihydrogen generation at an earlier time. This should occur since more excitons will be generated and therefore the necessary changes in morphology will result.

One more way to investigate suggested changes in morphology would be to increase the concentration of the CdSe-MSA•NafY•FeMo-co system by two or three fold, as long as the system could maintain solubility. The anticipated result would be that with the increases in concentration the dihydrogen would be progressively detected at earlier times because adequate changes in CdSe morphology would occur sooner because there were more CdSe nanoparticles to excite. The anticipated result would be dihydrogen generation at earlier times along with increasd amounts produced. . The explanation for hysteresis deserves further experimentation with the proper controls and variables.

Comparison of this Dihydrogen Production Method with Other Published Methods

The generation of dihydrogen from a sophisticated bioconjugate material such as CdSe-MSA•NafY•FeMoco is significant. To gauge how significant, the effectiveness of the system presented as part of the current study is compared to other published bioconjugate dihydrogen

generation methods (Table 2). The amount of dihydrogen or hydrocarbon production and the rates for the dihydrogen formation have been recalculated for direct comparisons. The first method combines CdTe nanoparticles with hydrogenase at a pH of 4.75 with ascorbic acid being the electron donor that produced dihydrogen at an impressive rate (93 nmol H_2/nmol active material/min). However, the reaction was only able to produce dihydrogen at this rate for five minutes, possibly due to degradation of the protein with the acidic conditions (*12*). The second method involved several MoFe proteins variants that allowed for conjugation of a $Ru(bypy)_2$ photosensitizer to one of three substituted cysteines near the bound FeMo-co. The system was able to produce 1.9 nmol H_2/nmol active material/min. The electron donor used was 200 mM dithionite and it was necessary that this excess be used to sustain the reaction for 50 minutes, which diminished in production after that point (*14*).

Table 2. Analytical Comparison of Different Dihydrogen Production Systems.

Method	*Rate of Production (H_2/nmol active material/minute	Maximum (nmol)	Time (min)	Ref	Reaction Conditions
CdTe/ Hydrogenase	93	70	5	5	pH 4.75
$Ru(bypy)_2$/ MoFe protein	1.9	2300	50	7	200 mM $Na_2S_2O_4$
**Eu^{II}-DTPA/ FeMo-co	0.097	5.8	60	59	
CdSe-MSA-NafY-FeMo-co	0.030	316	6840	this study	pH 8.0 2.0 mM $Na_2S_2O_4$

* Rates of production have been restated in equivalent units for comparison purposes.
** Ethylene production measured

Another method of not hydrogen production, but hydrocarbons production, is included since it uses FeMo-co. FeMo-co was combined with cyanide ion and europium (II) diethylenetriaminepentaacetate [Eu^{II}-DTPA], a strong photoactivated reductant. Hydrocarbons were produced with this system and more particularly ethene at 0.097/nmol H_2/nmol active material/min. The reaction was also attempted with carbon monoxide, but the hydrocarbons produced were considerably less. FeMo-co typically hydrolyzes in aqueous solvents, however, in this report it showed 85% activity after the first hour of being in an aqueous based solvent (*94*).

As seen in the table, the effectiveness of the CdSe-MSA•NafY•FeMo-co system for dihydrogen formation is comparable with the other reported systems. In terms of the rate of production, this system requires improvement to be competitive. However, this system is competitive enough, so that efforts expended towards increasing the amount produced and the rate of production are worthwhile. In terms of stability, the CdSe-MSA•NafY•FeMo-co system may have an advantage in that it was operational for 100 plus hours versus five minutes or one hour as with the other published systems. The length of time that the system is catalytically active could be a real plus as long as optimization of the system could increase the rate of dihydrogen production.

Potential Improvements for the CdSe•FeMo-co Systems

Ways to enhance the dihydrogen production using the CdSe-MSA•NafY•FeMo-co system include the following. The current systems were examined at a pH of 8.0. In the

aqueous CdSe-MSA•NafY•FeMo-co system, a feasible experiment would be to probe the limits of pH with respect to dihydrogen production, the stability of the system, and maintaining the solubility of the system. At lower pH values, the higher concentration of protons as substrates will drive the equilibrium forward. The method using CdTe-hydrogenase discussed earlier utilized a pH of 4.75 (*12*). Impressive dihydrogen production was observed, but only for five minutes. pH also plays a role in maintaining solubility with the CdSe-MSA. If the mercaptosuccinic acid is protonated, the result may be that the nanoparticles lose their ability to be aqueously solubilized. The pK_as of the carboxylic acid functional groups in mercaptosuccinic acid are pK_{a1} of 3.64 and pK_{a2} of 4.64. Consequently, any buffered solution in the pH range of 7.0 to 8.0 used to form the complex should maintain solubility. As seen with the CdSe-MSA•MoFe protein experiments, pH lower than 7.8 decreased the solubility of the system. There could have been more non-specific binding between the MoFe protein and the nanoparticle that could have contributed to diminished solubility. A study comparing solubility of the system compared to the protein with the FeMo-co (MoFe protein versus NafY protein), complexed to the CdSe-MSA would be beneficial to determine the size of the protein and its effects on solubility.

As mentioned earlier, the effects of decreasing pH from the presence of sodium dithionite and its hydrolysis could be a variable pertaining to the molar volume of dihydrogen produced. The effects of different sodium dithionite concentrations could be investigated. With an increase in the sodium dithionite, it will be important to combine the CdSe-MSA and NafY•FeMo-co at a lower concentration (0.2 sodium dithionite) as was done previously. This will give the complex adequate time to avoid competing effects from the dithionite for positions on the CdSe-MSA

surface. A validation that higher dithionite concentration may increase the amount of dihyrogen produced is found in the report that utilized the MoFe protein with bound $Ru(bypy)_2$. In that study, higher dithionite concentration, in a range from 20 mM to 200 mM, resulted in greater amounts of evolved dihydrogen corresponding to increased dithionite (*14*). The reaction with 200 mM dithionite produced a fivefold higher amount of dihydrogen produced compared to the 20 mM dithionite sample.

There are other experimental conditions or variables that could be investigated in order to optimize dihydrogen production. A different kind of nanoparticle could be synthesized and used as in the previous experiments such as cadmium telluride (CdTe). The bandgap energy of CdTe may be a closer match for the H_2/H^+ thermodynamic couple and FeMo-co's reduction potential. A study with various size of the same kind of nanoparticle could be conducted in order to ascertain any size dependent results for dihydrogen production. Other variables to explore in the dihydrogen generation experiments would be the kind of lamp used for illumination and temperature effects on the dihydrogen generation.

An interesting issue is the source of protons with the organic CdSe-TOP•FeMo-co system in chloroform. The 1 mM dithionite, 25 mM Tris solution in NMF solution with FeMo-co is the source of protons. With the addition of 5 μL of FeMo-co in NMF, 1 mM dithionite this equates to introducing 100 nanoliters of water to the sample. The one cuvette sample saw the production of 28 nmols of dihydrogen in one hour. How best to increase the source of protons in this system warrants further experimentation. The addition of pentafluorothiophenol ($C_6F_5S^-$) to FeMo-co was suggested as a source of protons catalytically, not as an ultimate source (*51*) The

$C_6F_5S^-$ replaces one of the amide ligands of the solvent NMF solution. Although the use of this ligand was inadequately explored in the previous study, it merits a thorough investigation.

This study described complexes formed between CdSe and FeMo-co in organic and in aqueous solvents and the experiments probing their interactions, along with their capability to produce dihyrogen when illuminated. While the experimental system studied here requires further optimization, it should to contribute to the pursuit of developing sustainable energy sources.

CHAPTER THREE: NIFEN PROTEIN AND ITS ROLE IN THE BIOSYNTHESIS OF THE IRON-MOLYBDENUM COFACTOR IN NITROGENASE

Introduction

Nitrogen fixation is essential for life and over one half of all global nitrogen fixation is performed by diazotrophic bacteria.(*95*) In these bacteria, the nitrogenase complex performs the reduction of dinitrogen to ammonia using the iron-molybdenum cofactor (FeMo-co), consisting of Fe_7MoS_9C−(*R*)-homocitrate.(*96*) The biosynthesis of FeMo-co is a complex process involving several enzymes, mostly encoded by nitrogen fixation (*nif*) genes. NifU and NifS synthesize smaller Fe_2S_2 and Fe_4S_4 type of clusters. NifB is thought to use the smaller Fe-S clusters to assemble a 6-Fe cluster termed as the NifB-cofactor.(*97*) This low molecular weight cofactor is then chaperoned to NifEN by NifX.(*98*) At this stage, the NifEN enzyme performs a complex multi-substrate reaction using NifB-co and incorporates molybdenum, homocitrate, and probably more Fe to complete the FeMo-co biosynthesis. The cluster is then chaperoned by NafY to the *apo*- form of the nitrogenase MoFeProtein component.(*99*)

The NifEN enzyme was first isolated by Dean and coworkers,(*55*) and studies in the last several years have shown the general reaction that it catalyzes. However, the exact enzymatic mechanism for this complicated, and important, reaction in FeMo-co biosynthesis is still largely unknown. NifEN likely performs the essential role of incorporating two additional components of FeMo-co, namely Mo and (*R*)-homocitrate, and possibly Fe and S. Molybdenum is provided to cultured bacteria as MoO_4^{2-}, with the Mo being in the +VI oxidation state, but it exists in the oxidation state of +IV in FeMo-co.(*100*) Hence, the MoO_4^{2-} oxoanion very likely undergoes a

two electron reduction during the process of FeMo-co synthesis. Free living diazotrophs such as *Azotobacter vinelandii*, in their natural niche, obtain their metals primarily from soil, where nearly all of Mo is in the form of molybdate, MoO_4^{2-}. It is the only oxoanion of molybdenum which is water soluble at neutral or slightly basic pH. Molybdenum uptake, metabolism, and activity are well studied topics in biology and provide significant insights towards the biological role of molybdenum.(*101-104*) The bacteria *A. vinelandii* sequester molybdenum using an ABC type of transport system.(*105*) These systems also help in being selective between Mo and W, since both the elements are present at comparable concentrations. However, the preferential uptake of W occurs in the absence of Mo and if W is available in sufficient concentration, resulting in ineffective nitrogen fixation. The ABC system is encoded by three genes, namely *modA*, *modB* and *modC*. The gene *modA* encodes for the molybdate binding protein located in the periplasm, *modB* encodes for a membrane protein that provides the transport channel and *modC* encodes for the protein that binds and hydrolyzes ATP to provide energy for active transport. This ABC transport system is essential for Mo metabolism and for diazotrophy in *A. vinelandii*, reflected by the presence of three copies of the *modABC* operon. The bacterium also has an astonishing ability to store molybdenum. It builds up 25 times more Mo than required for nitrogenase activity. Another protein associated with Mo storage in *A. vinelandii* is the Mo-storage protein (MoSto). MoSto provides molybdenum to nitrogenase especially when the cells are grown under Mo starvation conditions. A recent publication has characterized the protein's structure at 1.6 Å resolution and describes the compositions and structures of the various polyoxomolybdate clusters present in the protein.(*106*) In terms of FeMo-co biosynthesis in *A.vinelandii*, the *nifQ* gene product participates in Mo assimilation for FeMo-co synthesis(*107*)

and deletion of *nifQ* does impair diazotrophic growth at low MoO_4^{2-} concentrations. In addition to the NifQ protein, NifEN and NifH (FeProtein) are also required to incorporate molybdenum into FeMo-co.(*108, 109*) Thus MoO_4^{2-} is likely to be processed by the combined activities of NifEN and NifH for the Mo(VI) of MoO_4^{2-} to undergo a two electron reduction and the substitution of the oxygen ligands for sulfurs and homocitrate.

Previous FeMo-co biosynthesis experiments with radiolabeled ^{99}Mo showed association of ^{99}Mo with NifEN, and NifEN is highly likely to be required for chemical reduction and molybdenum incorporation to synthesize FeMo-co.(*109*) In this study, experiments are presented that better define the NifEN mechanism by indicating that NifEN acts as the molybdate reductase in FeMo-co biosynthesis.

Materials and Methods

Cell Growth.

The *A. vinelandii* strains DJ1041 and DJ884 were grown in a 100 L fermentor with modified Burke's media supplied with 10 mM urea as the nitrogen source at 30 °C.(*55, 110, 111*) After the cells reached an OD_{600} of 5, they were harvested and resuspended in 100 L of modified Burke's media with no fixed nitrogen. The cells were allowed to de-repress for four hours, then harvested and stored at -80 °C.

Protein Purification and Materials.

NifEN protein was purified from the *A. vinelandii* strain DJ1041 using a poly-His metal

affinity chromatography procedure described earlier.(*112*) FeProtein was purified from the *A. vinelandii* strain DJ884 using a published protocol.(*113*) All manipulations of protein were performed in septum-sealed serum vials under an O_2 free argon atmosphere using standard Schlenk line techniques or in a glove box comprising an atmosphere of nitrogen and 5% hydrogen. All liquid transfers were performed using gas tight syringes. Na_2MoO_4, Na_2WO_4, $MgCl_2$, ATP, $Na_2S_2O_4$ and trisodium (*R*)-homocitrate were used as supplied from Fisher or Sigma.

Sample Preparation for EPR.

Samples were made in 100 mM MOPS (pH 7.4) with 5 mM $Na_2S_2O_4$, 2 mM ATP, 100 μM NifEN, 400 μM Na_2MoO_4 and 400 μM (*R*)-homocitrate unless stated otherwise. To the above mixture, FeProtein (50 μM) was added and the mixture was allowed to incubate for 3 minutes at room temperature (*ca.* 23 °C) before being frozen in standard 3x4 mm EPR quartz tubes in liquid nitrogen. A hexanes-liquid nitrogen slush bath was used for flash-freezing samples.

X-Band EPR Spectroscopy.

X-band EPR spectra were recorded on a Bruker Elexsys E580 spectrometer equipped with an Oxford ESR900 helium flow cryostat and a Bruker standard rectangular TE102 resonator. The spectra were recorded at a modulation frequency of 100 kHz, modulation amplitude of 10 G, and a microwave frequency of approximately 9.45 GHz (with the precise

value recorded for each spectrum to ensure exact *g* alignment). All spectra were recorded at 9.5 K and a microwave power of 2.0 mW, with each trace being the sum of five scans, unless noted otherwise. The program IGOR Pro (WaveMetrics, Lake Oswego, OR) was used for all further treatment of the spectral data.

Results

A Mo-dependent EPR signal.

The dithionite reduced resting state of NifEN exhibits an $S = 1/2$ EPR signal, which may be axial or rhombic and possibly originate from more than a single species, with apparent *g* values of 2.07, 1.93, and 1.86. NifEN is thought to catalyze a reaction or process to append Fe, S, Mo, and possibly homocitrate to the 6-Fe complex NifB-co, the product of the NifB enzyme. However, the enzymological mechanistic understanding of the reaction catalyzed by NifEN has been lacking (Figure 17). To study the NifEN catalysis in relation to formation of FeMo-co, molybdate, homocitrate, ATP, and FeProtein were added to NifEN and the enzymatic reaction was inspected using EPR spectroscopy. A signal at $g = 2.00$ that overlaps the signal(s) for the Fe-S clusters of NifEN was observed for the reaction containing all reactants (Figure 18, trace 4). This Mo-dependent signal is observed only if all components of FeMo-co biosynthesis, *i.e.*, FeProtein, ATP, molybdate, and homocitrate are present. Absence of any of these components does not result in the signal at $g = 2.00$ (Figure 18). The spectra of the NifEN turnover sample with FeProtein, MgATP, and homocitrate, but without molybdate, is essentially an additive spectrum of the spectra for NifEN and FeProtein (Figure 18, trace 3). Subtraction of the

spectrum of the reaction lacking molybdate from the complete reaction shows a largely isotropic signal centered at g = 2.00 (Figure 18, trace 7).

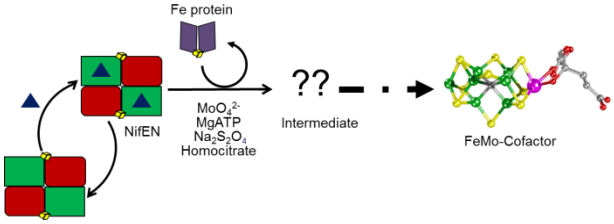

Figure 17. **Pathway of NifB-co to NifEN to FeMo-co**.
Schematic diagram showing the transformation of the NifB-co derived cluster (▲) of NifEN to FeMo-co. The yellow cubane represents a Fe4S4 cluster.

To positively identify NifEN as the enzyme performing the reaction on molybdate, control experiments were performed with NifEN omitted from the reaction. Without the NifEN protein, any concentration of the molybdate ions does not generate the signal at g = 2.00 (data not shown). This confirms that the FeProtein is not the enzyme responsible for the molybdate dependent signal or that the g = 2.00 signal is somehow generated due to a non-enzymatic process. Furthermore, the Mo-dependent signal is also not observed in the absence of FeProtein. ATP and homocitrate are also necessary for the generation of the molybdate dependent signal. The above observations clearly demonstrate that the new signal generated at g = 2.00 is a consequence of enzymatic turnover and not merely an adventitious chemical process.

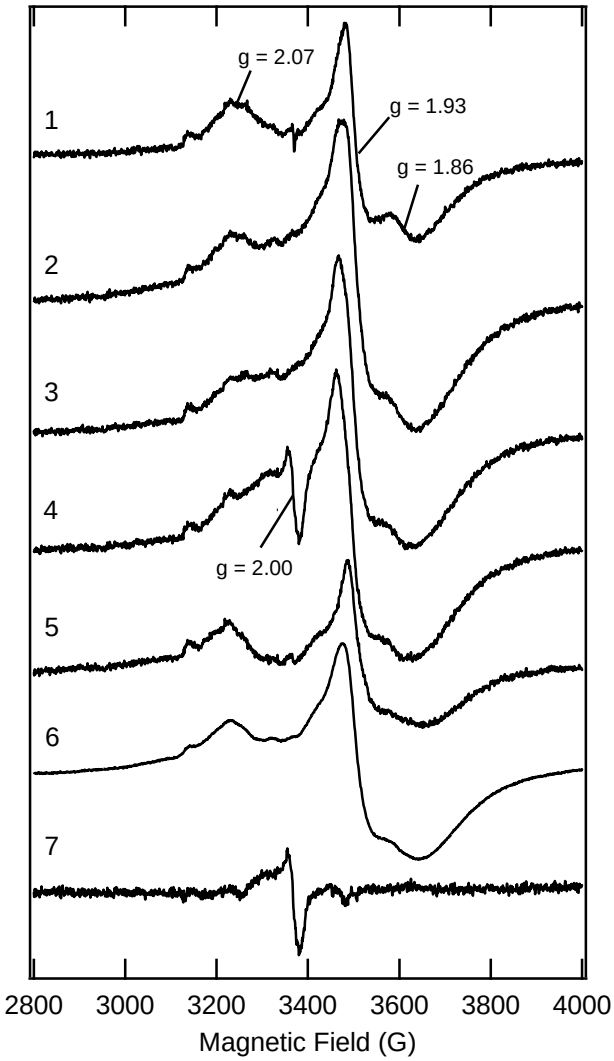

Figure 18. **EPR Spectra of Molybdate Turnover Samples Lacking Different Components.** EPR spectra of NifEN (trace 1), NifEN, NifH, and ATP (trace 2), NifEN, NifH, homocitrate, and ATP (trace 3), NifEN, NifH, molybdate, homocitrate, and ATP (trace 4), NifEN, molybdate, homocitrate, and ATP (trace 5), and NifEN, NifH, molybdate and ATP (trace 6). The signal at *g* = 2.00 was observed only in the presence of all components. All the mixtures were incubated for 3 minutes. Trace 7 exhibits the isotropic signal obtained from the subtraction of trace 3 from trace 4.

Given that the molybdate-dependent signal is observed at a *g*-value of 2.00, there exists the possibility that it is due to some non-specific Fe^{2+} or Fe^{3+} species. To ensure that the signal was not a result of an undesired Fe-S cluster degradation resulting in Fe^{2+} or Fe^{3+} ions, control

experiments were also performed by deliberately providing Fe^{3+} to the enzymatic mixture in the presence and absence of molybdate. In both cases, the signal at g = 2.00 was significantly less intense or negligible as compared to samples having the molybdate and without the added Fe^{3+} (Figure 19). The obvious correlation shown by the enzymes towards MoO_4^{2-} over Fe^{3+} proves that the signal is produced in a turnover-related process performed on the MoO_4^{2-} ion. We assign the isotropic signal at g = 2.00 to the reduction of an EPR silent Mo(VI) of MoO_4^{2-} to Mo(V), resulting in an EPR observable d^1 spin system.

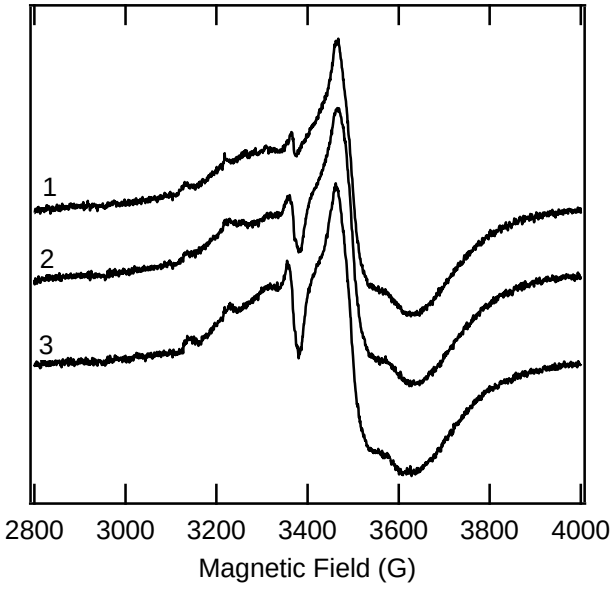

Figure 19. **EPR Spectra of NifEN Turnover Samples on Addition of MoO_4^{2-} and/or Fe^{3+} ions.**
EPR spectra with ferric and no molybdate (trace 1), with ferric and molybdate (trace 2), and only molybdate (trace 3) ions are shown. Both ferric and molybdate ions were added to a final concentration of 400 □M each. Concentrations for all other components are as described under Experimental Procedures.

Characterization of the Mo-dependent EPR signal.

The g = 2 region of the spectrum for the NifEN turnover reaction exhibits multiple overlapping S = 1/2 signals from NifEN and FeProtein thereby making this region somewhat complex to analyze. Temperature and power dependencies of these EPR signals were inspected to distinguish the molybdate dependent signal from those attributed to the Fe-S clusters of NifEN or FeProtein. Both the temperature and power profiles of the Mo-dependent signal (g = 2.00) are different than those of the NifEN signals (g = 1.93 and g = 2.07, Figures 20 and 21). The signals for NifEN with g-values of 1.93 and 2.07 are maximal at 7 K, whereas the molybdate-dependent signal at g = 2.00 increases in intensity to its maximum at 15 K followed by a decrease at higher temperatures of 18 K to 36 K, clearly having a different temperature maximum and profile. Also the power profile (Figure 21) of the different signals shows a markedly different behavior between the g = 2.00 signal when compared to the g = 1.93 and 2.07 signals. Hence the molybdate-dependent signal at g = 2.00 appears to have different spin saturation and relaxation properties and thus is truly distinct from the signals attributed to the Fe-S cluster(s) of NifEN.

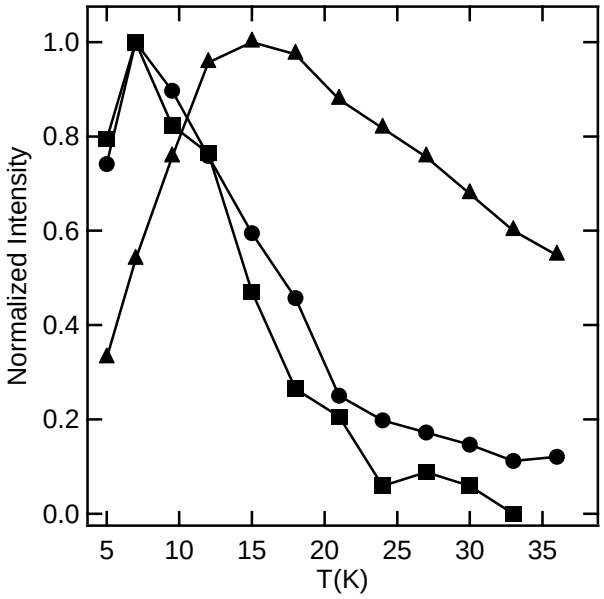

Figure 20. **Temperature Profile of EPR Signals.**
Signals at $g = 1.93$ (●), $g = 2.07$(■) and $g = 2.00$ (▲) for the molybdate-turnover sample. The peak intensities, relative to the maximal intensities are plotted against temperature at a microwave power of 0.63 mW.

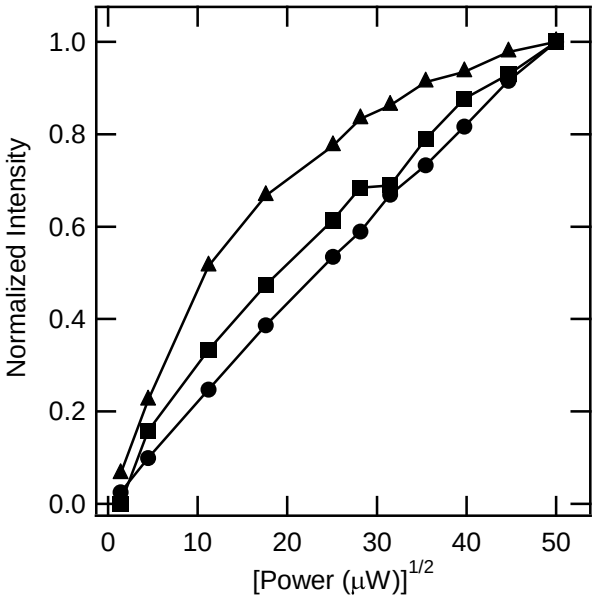

Figure 21. **Microwave Dependence of EPR Signals.**
Signals at $g = 1.93$ (●), $g = 2.07$(■) and $g = 2.00$ (▲) for the molybdate-turnover sample. The peak intensities, relative to the maximal intensities are plotted against the square root of microwave power at 12 K.

Reactant and inhibitor dependencies of the molybdate dependent g = 2.00 signal.

To fully attribute the g = 2.00 signal to be dependent on MoO_4^{2-}, a series of NifEN turnover reactions were prepared with increasing concentrations of MoO_4^{2-} as a reactant with constant concentrations of NifEN, FeProtein, MgATP, and homocitrate. An inspection of the EPR spectra of these samples shows a clear increase in the signal intensity for the signal at g = 2.00 with increasing concentrations of MoO_4^{2-} in the enzymatic reaction while no change is observed at g = 1.93 and g = 2.07. The plot of intensity against MoO_4^{2-} concentration shows saturating behavior, affirming that the signal is a consequence of a MoO_4^{2-} dependent enzymatic reaction (Figure 22).

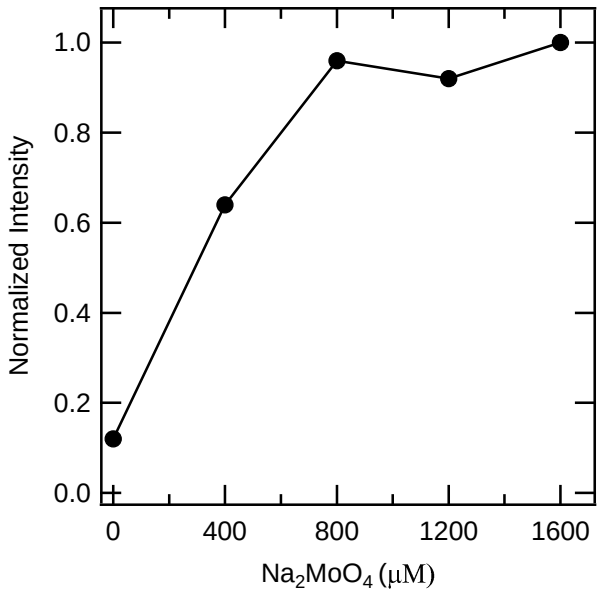

Figure 22. **Plot of Normalized Intensity for the g = 2.00 Signal with Respect to Molybdate.** Normalized intensity for the g = 2.00 signal with respect to amount of molybdate ions added to the enzymatic mixture. All samples were incubated for 3 minutes. Concentrations of NifEN and NifH were 70 μM and 35 μM respectively. The homocitrate concentration was kept constant at 400 μM.

If the moiety responsible for the g = 2.00 signal is a MoO_4^{2-} reduction intermediate, it is likely to be bound to the NifEN protein and not free in solution. To assess this point, an experiment using a membrane based separation was performed to further corroborate the dependence of the g = 2.00 signal on MoO_4^{2-} and that the Mo(V) species remains bound to the protein (Figure 23). A reaction was setup in a Centricon-30 (Millipore) with the same conditions as described above with all the required reaction constituents. The Centricon-30 was kept anaerobic and centrifuged to separate the high molecular weight proteinaceous components from the aqueous reaction solution in the filtrate containing only the low molecular weight components. Both the retentate and filtrate were inspected by EPR. The molybdate dependent g = 2.00 signal was only observed with the high molecular weight retentate and not in the filtrate or with the negative control samples lacking ATP. These observations indicate that the g = 2.00 related molybdenum species is bound to the protein and is not a free aqueous species.

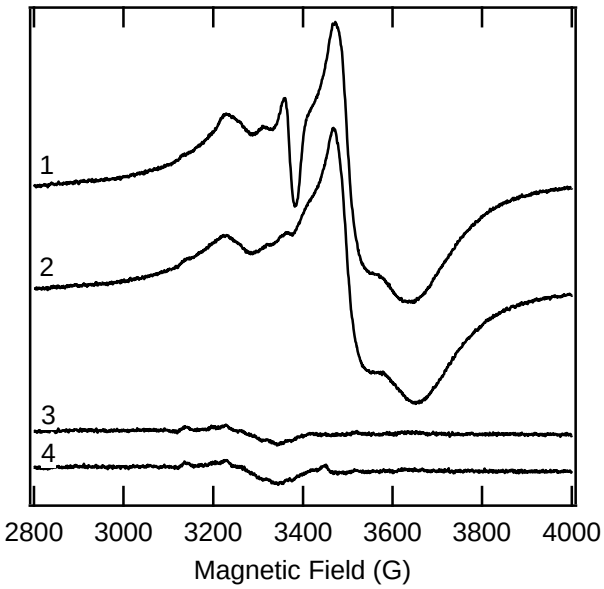

Figure 23. **EPR spectra of NifEN turnover samples.**
NifEN turnover samples and analogous controls when the samples were subjected to 30 kDa membrane filters post incubation. EPR spectra for the protein fractions of the turnover sample (trace 1) and corresponding control sample without ATP (trace 2) are shown. Traces 3 and 4 exhibit the signal from the buffer fractions of the turnover and corresponding control sample, respectively.

The effect of tungstate ions on nitrogenase expression, activity, and molybdenum uptake has been known for several decades.(*114-116*) Tungstate has also been shown to inhibit nitrogenase activity in diazotrophs.(*117*) ModA, the periplasmatic molybdate binding protein is incapable of distinguishing between the two oxoanions due to their similar sizes resulting in this competitive behavior.(*118*) Two reports using *A. vinelandii* and *Rhodobacter capsulatus* have exhibited the incorporation of tungsten in nitrogenase.*(119, 120)* In both these studies, W replaced Mo in the nitrogenase, partially in *A. vinelandii* and fully in *R. capsulatus*. The W-incorporated nitrogenases were purified from both bacteria and studied using EPR. Both show a $S = 3/2$ signal distinct from the FeMo-cofactor. In terms of activity, the 'tungsten nitrogenases'

show only marginal activity towards nitrogen and acetylene reduction but exhibit almost 25-30 % activity towards proton reduction as compared to the native MoFeProtein. Although tungstate is known to inhibit nitrogen fixation phenotype and nitrogenase activity, how exactly tungsten displaces molybdenum in FeMo-co has never been experimentally explored.

In our study, if the $g = 2.00$ signal is truly due to a molybdate dependent mechanism, reflective of Mo(VI) being reduced to Mo(V) as part of FeMo-co synthesis, competition with WO_4^{2-} ions should cause inhibition for binding of MoO_4^{2-} in a competitive manner and diminish the molybdate dependent signal. A series of turnover samples were prepared in the presence of increasing WO_4^{2-} concentration, with a fixed concentration of MoO_4^{2-} and inspected. As expected, a significant decrease in intensity of the signal at $g = 2.00$ was observed with increasing amounts of WO_4^{2-} ions (Figure 24). Hence, the WO_4^{2-} inhibits the molybdate reduction and further supports that the $g = 2.00$ signal is due to molybdate reduction.

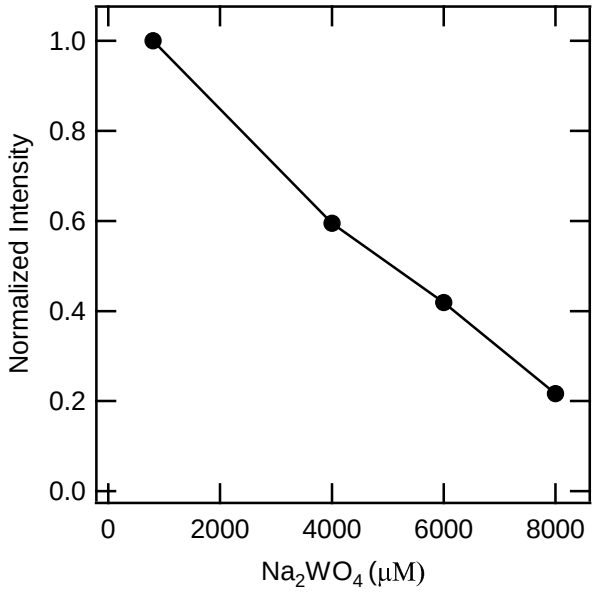

Figure 24. **Plot of Normalized Intensity.for the g = 2.00 signal with Respect to Tungstate.** Normalized intensity for the *g* = 2.00 signal with respect to amount of tungstate ions added to the enzymatic mixture. All samples were incubated for 3 minutes. Concentrations of NifEN and NifH were 70 μM and 35 μM respectively. Homocitrate and molybdate concentrations were kept constant at 800 μM.

(*R*)-homocitrate is also a co-substrate for the NifEN enzyme. In FeMo-co, (*R*)-homocitrate is bound to the Mo and both its exact role in nitrogenase catalysis and how it is incorporated is still unclear. Interestingly, homocitrate appears to be strictly required for the observation of the molybdate dependent *g* = 2.00 signal (Figure 2, trace 6). The homocitrate may be required in one or more ways of molybdate binding to NifEN, facilitation of reduction to the Mo(V) species, or stabilizing the reduced Mo(V) species.

Discussion

NifEN acts as a molybdate reductase.

NifEN performs the critical function in biological nitrogen fixation of using the 6-Fe NifB-co precursor as a substrate and likely incorporates additional Fe, S, Mo, and (*R*)-homocitrate to synthesize FeMo-co. Several reports have shown NifEN, when provided with MoO_4^{2-}, homocitrate, FeProtein, and ATP, to be capable of *in vitro* synthesis of FeMo-co and facilitation of MoFeProtein maturation measured by nitrogenase activity.(*121-123*) This is a complex bioinorganic reaction where multiple substrates and reaction components are utilized. Although this process has been investigated for some time, the biochemical understanding of the reaction mechanisms of this complex metallo-enzyme is still vague. The complexity of the NifEN based reaction makes it difficult to perform discrete biochemical analyses to define pertinent enzymological parameters such as substrate affinities, the stepwise binding of substrates, reaction order(s) and ultimate understanding of the chemical mechanism. For a large part, past work with NifEN has been phenomenological in most respects by assessing overall MoFeProtein maturation with nitrogenase activity assays,(*112*) or by changes in EPR lineshape, without rigorous analysis.(*122, 124*) In this work, an EPR signal is characterized, which is specifically associated with a single reactant of molybdate, and is ascribed to the reduction of molybdate-Mo(VI) to an EPR active Mo(V) species, relevant for its incorporation as part of FeMo-co.

Molybdenum is available to bacteria as MoO_4^{2-}, which is reduced and incorporated into FeMo-co as Mo(IV). Hence Mo(VI) in molybdate must undergo a minimum two electron

reduction during the synthesis of FeMo-co. The experiments described herein characterize a g = 2.00 EPR signal and ascribe it to the reduction of Mo(VI) to Mo(V). Experiments with appropriate controls described above show that the molybdate dependent g = 2.00 signal: (1) requires molybdate, FeProtein, NifEN, MgATP, and (*R*)-homocitrate; (2) is electronically distinct from EPR signals emanating from NifEN bound Fe-S clusters, based on distinct temperature and power profiles; (3) has a dependence on MoO_4^{2-} concentration and saturates; (4) is from a moiety bound to NifEN and not a free aqueous species; and (5) is diminished by inhibition with tungstate, which has been shown to abolish *nif* phenotype and can replace Mo in FeMo-co. All the above facts indicate that MoO_4^{2-}-Mo(VI) undergoes the reduction while being associated to NifEN.

As shown, the molybdate dependent g = 2.00 signal also requires turnover conditions with the nitrogenase FeProtein and MgATP. In nitrogenase, the FeProtein, bound with MgATP and its Fe_4S_4 cluster in the reduced 1+ state, docks to the MoFeProtein, MgATP is hydrolyzed concomitantly with the transfer of a single electron from the FeProtein-bound Fe_4S_4 cluster to the MoFeProtein, and this process is repeated for multiple cycles to amass sufficient electrons for the reduction of substrates.(*111*) While no experiment has directly shown electron transfer between FeProtein and NifEN, they are thought to function analogously to the nitrogenase complex and the FeProtein reduces metal cofactor components within NifEN. Thus, turnover of NifEN in conjunction with the MgATP hydrolysis dependent activity of FeProtein likely provides the electrons for the reduction of the molybdate. The molybdate-dependent g = 2.00 signal is only observed under such turnover condition with FeProtein and MgATP and is fitting with the reduction of molybdate-Mo(VI), which is EPR inactive, to an EPR active Mo(V) d^1 species.

Merely FeProtein, MgATP, and molybdate cannot perform molybdate reduction and do not produce the g = 2.0 signal. From the perspective of reducing capability, the FeProtein may be reductive enough to reduce Mo(VI) to Mo(V). The reduction potential for FeProtein when docked to the MoFeProtein is -350 mV *vs.* NHE.(*125*) Several literature reports for the reduction potential for the reduction of Mo(VI) to Mo(V) in biological systems indicate a value around -350 mV *vs.* NHE.(*126, 127*) Hence, the FeProtein - MoO_4^{2-} system may be able to perform the reduction of MoO_4^{2-}. However, the reduction indicated by the molybdate dependent g = 2.00 was observed only in the presence of NifEN, indicating that turnover related activity of the FeProtein provides the electron equivalence via NifEN.

As mentioned earlier, tungstate inhibits nitrogenase activity at the level of enzyme activity and nitrogen fixation at the phenotypic level, but the exact root of inhibition has never been explored. Geometrically, molybdenum and tungsten ions exhibit similar ionic radii due to lanthanide-contraction.(*128*) Tungstate's effect on nitrogenase activity can be explained by their ability to bind the NifEN enzyme, competitively against MoO_4^{2-}, owing to a similar size and shape as molybdate ions but not being reduced because of their more negative reduction potentials.(*119, 129*) Typically, W protein complexes differ from their molybdenum homologues by several hundred millivolts. Since, the reduction potential for FeProtein is close to Mo(VI), it is understandable that FeProtein may be incapable of reducing W(VI) to W(V) or to W(IV). The inhibition by WO_4^{2-} ions towards the formation of the g = 2.00 signal provides further evidence for the signal at g = 2.00 to be associated with molybdate.

Mo incorporation for FeMo-co synthesis.

The incorporation of Mo for the synthesis of FeMo-co is an obvious requirement and previous experiments have never conclusively defined the step where Mo is chemically incorporated as part of FeMo-co. Earlier experiments that utilized ^{99}Mo have implicated NifEN, NafY, NifX, and the nitrogenase FeProtein (NifH).(*108, 109*) The ^{99}Mo bound species are: ^{99}Mo containing FeMo-co, precursors of FeMo-co, or possibly intermediates bound to NifEN, NifX or NafY. ^{99}Mo in the context of a FeMo-co synthesis has been also found on the Fe-protein (NifH), but is likely to be ^{99}Mo-molybdate bound to the □-phosphoryl site of the MgATP site.

X-ray absorption spectroscopy (XAS) has previously identified Mo to be bound to NifEN. Examination of the "as purified" NifEN by Mo K-edge XAS has been performed.(*130*) The Mo site in NifEN when compared to the MoFeProtein exhibits a comparable oxidation state but dissimilar ligand field. In terms of Mo-O distances, the possibility of Mo=O was excluded. However, single bond Mo-O or Mo-N distances could not be assigned. The different ligand field for Mo in NifEN with respect to the MoFeProtein suggests that the Mo atom in NifEN is not part of the complete FeMo-co. The absence of Mo=O and a similar oxidation state in the MoFeProtein indicates that the Mo present in NifEN is in an oxidation state much lower than Mo(VI). A later report of Mo K-edge XAS of a NifEN after turnover with MoO_4^{2-} and MgATP-FeProtein largely concludes the same findings.(*122*)

Two other points regarding NifEN based molybdate reduction should be discussed here. First, the molybdate dependent g = 2.00 signal, likely from a Mo(V) species, appears to be largely isotropic and also electronically decoupled from the Fe-S cluster(s) of NifEN, which correlates with interpretations from the Mo K-edge XAS studies.(*122, 130*) This suggests that

possible further reduction may occur, maybe in conjunction with coupling to the NifB-co derived Fe-S precursor. Second, in our hands, the $g = 2.00$ signal indicating molybdate reduction is only observed in the presence of (*R*)-homocitrate, indicating that homocitrate is required: for either binding of molybdate to NifEN, for facilitation of reduction, or for stabilizing the Mo(V) species. This finding highly suggests that homocitrate is incorporated as part of FeMo-co at the NifEN step rather than at a later point. Further experiments are required to determine the relative affinities and the ordered sequence or randomness of binding for homocitrate and molybdate to NifEN.

The suggestion has previously been made that the Mo is introduced into FeMo-co at the NifEN step, but the experiments here have clearly shown that NifEN reduces molydate and that it likely facilitates reductive coupling of Mo to other parts that comprise FeMo-co. Considering that Mo probably is appended to a NifB-co derived Fe-S cluster, the 8-Fe model suggested for the NifEN bound Fe-S precursor(*131*) seems incongruent. An 8-Fe model for this bound intermediate would imply that an Fe atom be removed followed by inclusion of a Mo atom in NifEN during the biosynthesis of FeMo-co. There has been no experimental evidence, in terms of FeMo-co maturation assays, EPR spectroscopy, EXAFS, or XANES to indicate the decoupling of Fe atoms within NifEN. Determination of the X-ray diffraction structure for NifEN(*132*) is significant for understanding the NifEN protein structure, but it did not allow full resolution to precisely elucidate the structure of the bound Fe-S containing NifB-co derived FeMo-co precursor. Also the Fe *K*-edge EXAFS studies performed on NifEN exhibit no interactions of distances greater than 5 Å to substantiate(*131*) 1) interactions of the Fe core with an apical Fe atom and/or 2) interactions between two apical Fe atoms. Thus, the 8 Fe model

suggested for the NifB-co derived L cluster of NifEN seems unlikely.

Conclusion

The EPR based investigation of NifEN enzymatic reaction with FeProtein, MoO_4^{2-}, (*R*)-homocitrate, and MgATP allowed the characterization of a signal at $g = 2.00$. The signal was found to be dependent on MoO_4^{2-} and was observed only in the presence of all the components. The signal at $g = 2.00$ was assigned to a NifEN bound Mo(V) species formed from the reduction of MoO_4^{2-}. The results herein establish NifEN as the molybdate reductase for FeMo-co biosynthesis.

CHAPTER FOUR: CONCLUSIONS AND PERSPECTIVES ON DEVELOPING BETTER CATALYSTS TO PROVIDE ALTERNATIVE ENERGY RESOURCES

Introduction

Humanity is at a crossroads regarding how it provides energy for its needs. The fossil fuels that meet the majority of worldwide energy demands will run out perhaps in one or two generations. The real focus should be to marshal all scientific knowledge and innovation toward developing ways to generate adequate alternative fuels that will match and then exceed the current level of fossil fuel consumption. Toward the goal of developing alternative energy sources, this dissertation presented two major research efforts. First, development of a novel photo-activatable catalyst for production of dihydrogen was achieved by devising methods to complex cadmium selenide nanoparticles with FeMo-co, which was shown to effectively produce dihydrogen when illuminated with visible light. Second, EPR spectroscopic investigation of NifEN turnover samples in the process of FeMo-co biosynthesis showed a signal at $g = 2.00$. The signal at $g = 2.00$ was assigned to the reduction of Mo(VI) to Mo(V), thus identifying NifEN as a molybdate reductase. Both research efforts contribute toward developing better catalysts to enable production of new fuel sources.

The CdSe•FeMo-co Systems Developed to Photocatalytically Evolve Dihydrogen

To transduce energy of the visible light portion of the electro-magnetic spectrum into a fuel source, matching the band gap energy of a photo-active material near the thermodynamic

H^+/H_2 couple, with a corresponding reduction potential for the catalyst was necessary. First, the CdSe nanoparticles had to form a complex with the FeMo-co species. Fluorescence emission quenching of the CdSe demonstrated the formation of a complex in both the CdSe-TOP●FeMo-co system in chloroform and the CdSe-MSA●NafY●FeMo-co system in aqueous solvent. To potentiate efficient electron transfer, the formation of a complex between CdSe and FeMo-co was required.

EPR based inspection of the CdSe-TOP●FeMo-co system showed a $g \sim 2$ signal that is indicative of an $S = 1/2$ spin state and suggests an electronic change in FeMo-co when complexed to CdSe-TOP. The aqueous CdSe●NafY●FeMo-co system showed minimal change in the $S = 3/2$ spin state initially, interpreted as the complex formation not perturbing the FeMo-co. After intense illumination, a diminished EPR species with the same line shape as the $S = 3/2$ spin state seen prior to illumination. The diminishment in signal intensity corresponds to a change in the $S = 3/2$ spin state population to some other EPR silent state. The interpretation was that the photo-activated CdSe-MSA participated in an electron transfer to FeMo-co.

The capability of the CdSe-MSA●NafY●FeMo-co system for generating dihydrogen for a period of 100 plus hours was demonstrated. The following factors contributed to the positive result affirming the project hypothesis. The system was aqueous with a ready source of protons available for reduction. The longevity of the NafY●FeMo-co complexed to a photo-active material staying intact and performing catalysis for four to five days is rare in the literature for a bioconjugate type of material.

Investigation of NifEN's Role as a Molybdate Reductase

EPR based inspection of NifEN enzyme turnover samples showed a signal at $g = 2.00$ observed only if all the substrates necessary for turnover were present. The signal at $g = 2.00$ was found to be molybdate concentration dependent. The molybdenum in molybdate, the oxoanion source of molybdenum for organisms, is in an oxidation state of (VI). The molybdenum in FeMo-co is in an oxidation state of (IV). The hypothesis was that the $g = 2.00$ signal was associated with the reduction of molybdenum so as to enable its insertion into the FeMo-co precursor inside NifEN protein.

Temperature and power profiles of the $g = 2.00$ signal compared to the signals at $g = 1.93$ and $g = 2.07$ associated with the Fe-S clusters of NifEN indicated a distinct species apart from the Fe-S clusters of NifEN clusters. A centrifugal ultrafiltration experiment confirmed that the species associated with the $g = 2.00$ signal was bound to NifEN and not in solution. Tungstate inhibition was demonstrated when the species associated with the $g = 2.00$ signal were diminished as increasing amounts of tungstate were added to the enzyme turnover samples. There was no evidence that the $g = 2.00$ signal arose from ferric irons in solution from oxidation of the system, or from the action of NifH alone. Based on these results, the $g = 2.00$ signal was assigned to the reduction of Mo(VI) to Mo(V), thus identifying NifEN as a molybdate reductase. A key step in the complicated biosynthetic pathway of FeMo-co has been better elucidated. With further studies, the goal of developing a biomimetic FeMo-co catalyst is closer to reality.

Towards Development of Alternative Energy Resources

NifEN's Role as a Molybdate Reductase.

A better understanding of how Nature synthesizes catalysts will lead toward mimicking these catalysts and their properties. The work with NifEN expands the understanding of the FeMo-co biosynthetic pathway. A biomimetic catalyst could replace the Fe catalyst and allow for decreasing the high temperatures and pressures used in the Haber-Bosch process, thus lowering the energy demands for the process. Furthermore, a biomimetic material could be used to catalyze dihydrogen production. The knowledge gained regarding the formation of biological catalysts, can impact the study and investigation of other intriguing systems.

CdSe-MSA•NafY•FeMo-co system.

The central goal of this study was to develop better catalysts for alternative fuels, therefore the focus of future research should be to optimize and scale up dihydrogen production for industrial application purposes. The most obvious variable to investigate is the pH. More protons available for reduction should increase the rate since the CdSe-MSA•NafY•FeMo-co system has proven to be catalytic. There is a limit to the pH values that can be investigated based on the stability and solubility of the CdSe-MSA•NafY•FeMo-co system.

Investigation of the optimal nanoparticle size for complex formation can be justified. The NafY-FeMo-co system is approximately 15 nanometers in length (*90*). The nanoparticle diameter was determined to be 2.4 nanometers in diameter and is considered to be somewhat spherical in shape. The nanoparticle diameter used in this study was calculated using an

extinction coefficient based on a first peak absorbance (*133*). The surface area on the nanoparticle required for adequate complex formation with either NafY●FeMo-co or FeMo-co (8 to 10 Angstroms (*71*)) to facilitate electron transfer could be explored with an investigation with various nano-particle sizes. The effectiveness to either generate dihydrogen or cause electron transfer investigated by EPR could be examined to determine the optimal diameter of CdSe to form the complex with the FeMo-co species.

A higher band gap material used in the same set of experiments could increase rate of dihydrogen production and the amount of dihydrogen produced overall. Higher band gap energy corresponds to greater photo-activity and therefore more efficient electron transfer rather than the electron relaxing back to the ground state (*134*). Core quantum dots coated with higher band gap material shells have demonstrated greater quantum yield, improved photo-stability and increased photo-activity. An example is a core CdSe coated with either with a ZnS or a CdS shell. Passivation of the surface trap states by the shell and confinement of the exciton to the core are thought to be the reasons for the overall enhancement of photo-activity. Their use may result in greater dihydrogen production at faster rates (*135*).

Different intensities of light could be investigated. The increase of flux could possibly create more excited electrons per unit of time. Intensity is measured in lumens per sterdian; also expressed as number of photons bombarding on a unit area. Intuitively, this would result in more excited electrons and therefore a greater number of electron transfers (*136*), thus increasing the rate of dihydrogen production.

Dithionite concentration effects could be investigated. In the MoFe protein conjugated to $Ru(bypy)_2$ at the active site near FeMo-co, an increase of dithionite concentration resulted in

greater amount of diydrogen production (*14*). The increase of dithionite concentration coinciding with increased diydrogen production could happen for several reasons. The dithionite is known as an effective oxygen scavenger to preserve the anaerobic environment necessary for FeMo-co stablility (*71*). The dithionite is a reductant and serves to fill the electron hole generated with formation of the exciton (*14*). The $SO_2^{\cdot -}$ radical that is the real reductant can possibly react with water to form $H^{+\cdot}$ and thus increase the source of protons (*137*).

An additional aspect to dithioinite use is the fact that the catalysis perfomed by FeMo-co is a sustained reductive catalysis. The oxidation of dithionte with the concomitant formation of the $SO_2^{\cdot -}$ radical could possibly degrade FeMo-co. However, the presence of FeMo-co inside NafY provides protection for the Fe-S cluster. The use of NafY●FeMo-co in other catalytic systems is worth exploring.

The dithionite issues are interesting with respect to the longevity of the CdSe-MSA●NafY●FeMo-co performing catalysis for 100 plus hours. Was it that the dithionite source was depleted and no longer able to be the electron donor for the electron hole generated with the photo-activated exciton generation? Or was it that the dithionite was depleted and the formation of the $SO_2^{\cdot -}$ radical able to condense with water thereby decreasing the pH was diminished, thus decreasing the source of H^+? Would the longevity of the NafY●FeMo-co system be extended beyond 4 to 5 days if dithionite concentrations were increased? Would changes in pH, with or without the adjustments in dithionite concentration, enhance the observed longevity of the system to enable continuation of catalysis? All these questions could be explored with dithionite dependent and pH dependent studies. Also, after a one hundred hour experiment, detection of

the pH and FeMo-co activity nitrogenase assay would be important data to contribute to longevity investigations.

One other aspect of dithionite use is worth mentioning. The dithionite reagent is not inexpensive. The use of other typical reductants used in biological applications could be investigated. The reduction potentials of some of these reagents are as follows: 1) dithionite, -0.45 V (*138*), 2) mercaptoethanol, -0.26 V (*30*), 3) dithiothreitol, -0.33 V (*139*), 4) glutathione, -0.27 V (*140*), 5) methyl viologen, -0.44 V, 6) benzyl viologen, -0.36 V and 7) flavinmononucleotide, -0.24 V (*67*) When compared to the reduction potential of FeMo-co , -0.46 V (*40*), the only reductants able to reduce FeMo-co are dithionite and methyl viologen. This effort merits further investigation.

The ways to improve dihydrogen generation presented here have been in regards to the CdSe-MSA●NafY●FeMo-co so far. The CdSe-TOP●FeMo-co system merits investigation because of the higher quantum yields associated with nanoparticles dissolved in organic solvents as compared to aqueous solubilized nanoparticles. From the observed fluorescence emission quenching of CdSe-TOP, complex formation between it and FeMo-co was demonstrated. EPR spectroscopic investigation of the CdSe-TOP●FeMo-co system suggested an electron transfer. The CdSe-TOP●FeMo-co system when illuminated could possibly evolve dihydrogen.

The FeMo-co in the CdSe-TOP FeMo-co system is more labile because it lacks the protection of a protein. Nonetheless, the system is worth investigating because of the high photo-activity of organically soluble CdSe-TOP nanoparticles. FeMo-co dissolved in NMF is miscible with chloroform. An issue to explore would be the stability of the CdSe-TOP●FeMo-co system. There would also be a need to increase the source of protons in the system.

A photo-activated CdSe●FeMo-co system has demonstrated passive production of dihydrogen. There are numerous options that could be investigated for the purpose of optimization of the dihydrogen production systems. Could a system be set up to drive other photo-activated reactions? Could MoFe protein be complexed with a photo-active material to possibly perform nitrogen fixation? The nanoparticle would be replacing the function of the Fe protein (¯0.12 to ¯0.30 to ¯0.46 V (*141, 142*)) so it might require a greater bandgap energy nanoparticle; CdSe nanoparticle's band gap energy may not be adequate. This development would be a greener approach compared to the current Haber-Bosch process with its high energy demands.

The CdSe-TOP●FeMo-co systems showed evidence of electron transfer. The CdSe MSA●NafY●FeMo-co showed dihydrogen generation. Both CdSe systems complexed to a FeMo-co species merit further study and optimization. The NifEN role as a molybdenum reductase has been demonstrated and will contribute to a better understanding of the FeMo-co biosynthetic pathway. These studies will further humankind's development of renewable energy sources.

REFERENCES

1. (2005) Act locally, trade globally emissions trading for climate policy, p 1 online resource (234 p., International Energy Agency,, Paris.

2. Huber, W., and Kolb, G. (1995) Life-Cycle Analysis of Silicon-Based Photovoltaic Systems, *Solar Energy 54*, 153-163.

3. Smil, V. (2002) Nitrogen and food production: proteins for human diets, *Ambio 31*, 126-131.

4. Iyngaran, P., Madden, D. C., Jenkins, S. J., and King, D. A. (2011) Hydrogenation of N over Fe{111}, *Proc Natl Acad Sci U S A 108*, 925-930.

5. Fujishima, A., and Honda, K. (1972) Electrochemical photolysis of water at a semiconductor electrode, *Nature 238*, 37-38.

6. Kudo, A., and Miseki, Y. (2009) Heterogeneous photocatalyst materials for water splitting, *Chem Soc Rev 38*, 253-278.

7. Service, R. F. (2011) Chemistry. Artificial leaf turns sunlight into a cheap energy source, *Science 332*, 25.

8. Nocera, D. G. (2012) The Artificial Leaf, *Acc Chem Res*.

9. Vincent, K. A., Parkin, A., and Armstrong, F. A. (2007) Investigating and exploiting the electrocatalytic properties of hydrogenases, *Chem Rev 107*, 4366-4413.

10. Igarashi, R. Y., and Seefeldt, L. C. (2003) Nitrogen fixation: the mechanism of the Mo-dependent nitrogenase, *Crit Rev Biochem Mol Biol 38*, 351-384.

11. Masukawa, H., Zhang, X. H., Yamazaki, E., Iwata, S., Nakamura, K., Mochimaru, M., Inoue, K., and Sakurai, H. (2009) Survey of the Distribution of Different Types of Nitrogenases and Hydrogenases in Heterocyst-Forming Cyanobactera, *Marine Biotechnology 11*, 397-409.

12. Brown, K. A., Dayal, S., Ai, X., Rumbles, G., and King, P. W. (2010) Controlled assembly of hydrogenase-CdTe nanocrystal hybrids for solar hydrogen production, *J Am Chem Soc 132*, 9672-9680.

13. Reisner, E., Powell, D. J., Cavazza, C., Fontecilla-Camps, J. C., and Armstrong, F. A. (2009) Visible light-driven H(2) production by hydrogenases attached to dye-sensitized TiO(2) nanoparticles, *J Am Chem Soc 131*, 18457-18466.

14. Roth, L. E., Nguyen, J. C., and Tezcan, F. A. (2010) ATP- and iron-protein-independent activation of nitrogenase catalysis by light, *J Am Chem Soc 132*, 13672-13674.

15. Murray, C. B., Norris, D. J., and Bawendi, M. G. (1993) Synthesis and Characterization of Nearly Monodisperse Cde (E = S, Se, Te) Semiconductor Nanocrystallites, *J Am Chem Soc 115*, 8706-8715.

16. Qu, L., and Peng, X. (2002) Control of photoluminescence properties of CdSe nanocrystals in growth, *J Am Chem Soc 124*, 2049-2055.

17. Nozik, A. J. (2001) Spectroscopy and hot electron relaxation dynamics in semiconductor quantum wells and quantum dots, *Annual Review of Physical Chemistry 52*, 193-231.

18. Peng, X. G., Wickham, J., and Alivisatos, A. P. (1998) Kinetics of II-VI and III-V colloidal semiconductor nanocrystal growth: "Focusing" of size distributions, *J Am Chem Soc 120*, 5343-5344.

19. Biju, V., Itoh, T., Anas, A., Sujith, A., and Ishikawa, M. (2008) Semiconductor quantum dots and metal nanoparticles: syntheses, optical properties, and biological applications, *Anal Bioanal Chem 391*, 2469-2495.

20. Kamat, P. V. (2008) Quantum Dot Solar Cells. Semiconductor Nanocrystals as Light Harvesters, *Journal of Physical Chemistry C 112*, 18737-18753.

21. Murray, C. B., and Bawendi, M. G. (1993) Synthesis and Physical Characterization of Ii-Vi-Semiconductor Nanocrystallites (Quantum Dots), *Abstracts of Papers of the American Chemical Society 205*, 136-PHYS.

22. Peng, X., Manna, L., Yang, W., Wickham, J., Scher, E., Kadavanich, A., and Alivisatos, A. P. (2000) Shape control of CdSe nanocrystals, *Nature 404*, 59-61.

23. Matylitsky, V. V., Dworak, L., Breus, V. V., Basche, T., and Wachtveitl, J. (2009) Ultrafast charge separation in multiexcited CdSe quantum dots mediated by adsorbed electron acceptors, *J Am Chem Soc 131*, 2424-2425.

24. Mahler, B., Spinicelli, P., Buil, S., Quelin, X., Hermier, J. P., and Dubertret, B. (2008) Towards non-blinking colloidal quantum dots, *Nat Mater 7*, 659-664.

25. Mohamed, M. B., Tonti, D., Al-Salman, A., Chemseddine, A., and Chergui, M. (2005) Synthesis of high quality zinc blende CdSe nanocrystals, *J Phys Chem B 109*, 10533-10537.

26. Winter, J. O., Gomez, N., Gatzert, S., Schmidt, C. E., and Korgel, B. A. (2005) Variation of cadmium sulfide nanoparticle size and photoluminescence intensity with altered

aqueous synthesis conditions, *Colloids and Surfaces a-Physicochemical and Engineering Aspects 254*, 147-157.

27. Zhou, C., Shen, H., Guo, Y., Xu, L., Niu, J., Zhang, Z., Du, Z., Chen, J., and Li, L. S. (2010) A versatile method for the preparation of water-soluble amphiphilic oligomer-coated semiconductor quantum dots with high fluorescence and stability, *J Colloid Interface Sci 344*, 279-285.

28. Kloepfer, J. A., Bradforth, S. E., and Nadeau, J. L. (2005) Photophysical properties of biologically compatible CdSe quantum dot structures, *Journal of Physical Chemistry B 109*, 9996-10003.

29. Zhelev, Z., Bakalova, R., Ohba, H., Jose, R., Imai, Y., and Baba, Y. (2006) Uncoated, broad fluorescent, and size-homogeneous CdSe quantum dots for bioanalyses, *Anal Chem 78*, 321-330.

30. Nelcon, D. R., Lehninger ,Albert L, Cox, Michael (2005) *Lehninger principles of biochemistry*, W. H. Freeman, New York.

31. Chan, M. K., Kim, J., and Rees, D. C. (1993) The nitrogenase FeMo-cofactor and P-cluster pair: 2.2 A resolution structures, *Science 260*, 792-794.

32. Lancaster, K. M., Roemelt, M., Ettenhuber, P., Hu, Y., Ribbe, M. W., Neese, F., Bergmann, U., and DeBeer, S. (2011) X-ray emission spectroscopy evidences a central carbon in the nitrogenase iron-molybdenum cofactor, *Science 334*, 974-977.

33. Einsle, O., Tezcan, F. A., Andrade, S. L., Schmid, B., Yoshida, M., Howard, J. B., and Rees, D. C. (2002) Nitrogenase MoFe-protein at 1.16 A resolution: a central ligand in the FeMo-cofactor, *Science 297*, 1696-1700.

34. Mulder, D. W., and Peters, J. W. (2011) Small angle x-ray scattering spectroscopy, *Methods Mol Biol 766*, 177-189.

35. Lukoyanov, D., Yang, Z. Y., Barney, B. M., Dean, D. R., Seefeldt, L. C., and Hoffman, B. M. (2012) Unification of reaction pathway and kinetic scheme for N2 reduction catalyzed by nitrogenase, *Proc Natl Acad Sci U S A 109*, 5583-5587.

36. Seefeldt, L. C., Hoffman, B. M., and Dean, D. R. (2012) Electron transfer in nitrogenase catalysis, *Curr Opin Chem Biol 16*, 19-25.

37. Wink, D. A., McLean, P. A., Hickman, A. B., and Orme-Johnson, W. H. (1989) A new method for extraction of iron-molybdenum cofactor (FeMoco) from nitrogenase adsorbed to DEAE-cellulose. 2. Solubilization of FeMoco in a wide range of organic solvents, *Biochemistry 28*, 9407-9412.

38. Cramer, S. P., Gillum, W. O., Hodgson, K. O., Mortenson, L. E., Stiefel, E. I., Chisnell, J. R., Brill, W. J., and Shah, V. K. (1978) Molybdenum Site of Nitrogenase .2. Comparative-Study of Mo-Fe Proteins and Iron-Molybdenum Cofactor by X-Ray Absorption Spectroscopy, *J Am Chem Soc 100*, 3814-3819.

39. Shah, V. K., and Brill, W. J. (1977) Isolation of an iron-molybdenum cofactor from nitrogenase, *Proc Natl Acad Sci U S A 74*, 3249-3253.

40. Burgess, B. K., Stiefel, E. I., and Newton, W. E. (1980) Oxidation-reduction properties and complexation reactions of the iron-molybdenum cofactor of nitrogenase, *J Biol Chem 255*, 353-356.

41. Burgess, B. K. (1990) The Iron Molybdenum Cofactor of Nitrogenase, *Chemical Reviews 90*, 1377-1406.

42. Walters, M. A., Chapman, S. K., and Ormejohnson, W. H. (1986) The Nature of Amide Ligation to the Metal Sites of Femoco, *Polyhedron 5*, 561-565.

43. Schultz, F. A., Gheller, S. F., Burgess, B. K., Lough, S., and Newton, W. E. (1985) Electrochemical Characterization of the Iron Molybdenum Cofactor from Azotobacter-Vinelandii Nitrogenase, *J Am Chem Soc 107*, 5364-5368.

44. Rawlings, J., Shah, V. K., Chisnell, J. R., Brill, W. J., Zimmermann, R., Munck, E., and Orme-Johnson, W. H. (1978) Novel metal cluster in the iron-molybdenum cofactor of nitrogenase. Spectroscopic evidence, *J Biol Chem 253*, 1001-1004.

45. Hedman, B., Frank, P., Gheller, S. F., Roe, A. L., Newton, W. E., and Hodgson, K. O. (1988) New Structural Insights into the Iron Molybdenum Cofactor from Azotobacter-Vinelandii Nitrogenase through Sulfur-K and Molybdenum-L X-Ray Absorption-Edge Studies, *J Am Chem Soc 110*, 3798-3805.

46. Conradson, S. D., Burgess, B. K., and Holm, R. H. (1988) Fluorine-19 chemical shifts as probes of the structure and reactivity of the iron-molybdenum cofactor of nitrogenase, *J Biol Chem 263*, 13743-13749.

47. Conradson, S. D., Burgess, B. K., Newton, W. E., Hodgson, K. O., Mcdonald, J. W., Rubinson, J. F., Gheller, S. F., Mortenson, L. E., Adams, M. W. W., Mascharak, P. K., Armstrong, W. A., and Holm, R. H. (1985) Structural Insights from the Mo K-Edge X-Ray Absorption near Edge Structure of the Iron Molybdenum Protein of Nitrogenase and Its Iron Molybdenum Cofactor by Comparison with Synthetic Fe-Mo-S Clusters, *J Am Chem Soc 107*, 7935-7940.

48. Liu, H. B. I., Filipponi, A., Gavini, N., Burgess, B. K., Hedman, B., Dicicco, A., Natoli, C. R., and Hodgson, K. O. (1994) Exafs Studies of Femo-Cofactor and Mofe Protein -

Direct Evidence for the Long-Range Mo-Fe-Fe Interaction and Cyanide Binding to the Mo in Femo-Cofactor, *J Am Chem Soc 116*, 2418-2423.

49. Richards, A. J., Lowe, D. J., Richards, R. L., Thomson, A. J., and Smith, B. E. (1994) Electron-paramagnetic-resonance and magnetic-circular-dichroism studies of the binding of cyanide and thiols to the thiols to the iron-molybdenum cofactor from Klebsiella pneumoniae nitrogenase, *Biochem J 297 (Pt 2)*, 373-378.

50. Ibrahim, S. K., Vincent, K., Gormal, C. A., Smith, B. E., Best, S. P., and Pickett, C. J. (1999) The isolated iron-molybdenum cofactor of nitrogenase binds carbon monoxide upon electrochemically accessing reduced states, *Chemical Communications*, 1019-1020.

51. Le Gall, T., Ibrahim, S. K., Gormal, C. A., Smith, B. E., and Pickett, C. J. (1999) The isolated iron-molybdenum cofactor of nitrogenase catalyses hydrogen evolution at high potential, *Chemical Communications*, 773-774.

52. Pickett, C. J., Vincent, K. A., Ibrahim, S. K., Gormal, C. A., Smith, B. E., and Best, S. P. (2003) Electron-transfer chemistry of the iron-molybdenum cofactor of nitrogenase: delocalized and localized reduced states of FeMoco which allow binding of carbon monoxide to iron and molybdenum, *Chemistry 9*, 76-87.

53. Pickett, C. J., Vincent, K. A., Ibrahim, S. K., Gormal, C. A., Smith, B. E., Fairhurst, S. A., and Best, S. P. (2004) Synergic binding of carbon monoxide and cyanide to the FeMo cofactor of nitrogenase: relic chemistry of an ancient enzyme?, *Chemistry 10*, 4770-4776.

54. Curatti, L., Hernandez, J. A., Igarashi, R. Y., Soboh, B., Zhao, D., and Rubio, L. M. (2007) In vitro synthesis of the iron-molybdenum cofactor of nitrogenase from iron, sulfur, molybdenum, and homocitrate using purified proteins, *Proc Natl Acad Sci U S A 104*, 17626-17631.

55. Goodwin, P. J., Agar, J. N., Roll, J. T., Roberts, G. P., Johnson, M. K., and Dean, D. R. (1998) The *Azotobacter vinelandii* NifEN complex contains two identical [4Fe-4S] clusters, *Biochemistry 37*, 10420-10428.

56. Rubio, L. M., Singer, S. W., and Ludden, P. W. (2004) Purification and characterization of NafY (apodinitrogenase gamma subunit) from Azotobacter vinelandii, *J Biol Chem 279*, 19739-19746.

57. Hernandez, J. A., Phillips, A. H., Erbil, W. K., Zhao, D., Demuez, M., Zeymer, C., Pelton, J. G., Wemmer, D. E., and Rubio, L. M. (2011) A sterile alpha-motif domain in NafY targets apo-NifDK for iron-molybdenum cofactor delivery via a tethered domain, *J Biol Chem 286*, 6321-6328.

58. International Energy Agency. (2008) *Deploying renewables : principles for effective policies*, International Energy Agency, Paris.

59. Tvrdy, K., and Kamat, P. V. (2009) Substrate Driven Photochemistry of CdSe Quantum Dot Films: Charge Injection and Irreversible Transformations on Oxide Surfaces, *Journal of Physical Chemistry A 113*, 3765-3772.

60. Rees, D. C., Akif Tezcan, F., Haynes, C. A., Walton, M. Y., Andrade, S., Einsle, O., and Howard, J. B. (2005) Structural basis of biological nitrogen fixation, *Philos Transact A Math Phys Eng Sci 363*, 971-984; discussion 1035-1040.

61. Lancaster, K. M., Roemelt, M., Ettenhuber, P., Hu, Y. L., Ribbe, M. W., Neese, F., Bergmann, U., and DeBeer, S. (2011) X-ray Emission Spectroscopy Evidences a Central Carbon in the Nitrogenase Iron-Molybdenum Cofactor, *Science 334*, 974-977.

62. Seefeldt, L. C., Hoffman, B. M., and Dean, D. R. (2009) Mechanism of Mo-dependent nitrogenase, *Annu Rev Biochem 78*, 701-722.

63. Seefeldt, L. C., Rasche, M. E., and Ensign, S. A. (1995) Carbonyl sulfide and carbon dioxide as new substrates, and carbon disulfide as a new inhibitor, of nitrogenase, *Biochemistry 34*, 5382-5389.

64. Sakurai, H., and Masukawa, H. (2007) Promoting R & D in photobiological hydrogen production utilizing mariculture-raised cyanobacteria, *Marine Biotechnology 9*, 128-145.

65. Watanabe, T., and Honda, K. (1982) Measurement of the Extinction Coefficient of the Methyl Viologen Cation Radical and the Efficiency of Its Formation by Semiconductor Photocatalysis, *Journal of Physical Chemistry 86*, 2617-2619.

66. Yu, W. W., Qu, L. H., Guo, W. Z., and Peng, X. G. (2003) Experimental determination of the extinction coefficient of CdTe, CdSe, and CdS nanocrystals, *Chemistry of Materials 15*, 2854-2860.

67. Christiansen, J., Goodwin, P. J., Lanzilotta, W. N., Seefeldt, L. C., and Dean, D. R. (1998) Catalytic and biophysical properties of a nitrogenase Apo-MoFe protein produced by a nifB-deletion mutant of Azotobacter vinelandii, *Biochemistry 37*, 12611-12623.

68. Laemmli, U. K. (1970) Cleavage of Structural Proteins during Assembly of Head of Bacteriophage-T4, *Nature 227*, 680-&.

69. Lowry, O. H., Rosebrough, N. J., Farr, A. L., and Randall, R. J. (1951) Protein measurement with the Folin phenol reagent, *J Biol Chem 193*, 265-275.

70. Van de Bogart, M., and Beinert, H. (1967) Micro methods for the quantitative determination of iron and copper in biological material, *Anal Biochem 20*, 325-334.

71. Burgess, B. K. (1990) The Iron Molybdenum Cofactor of Nitrogenase, *Chem Rev 90*, 1377-1406.

72. Smith, P. K., Krohn, R. I., Hermanson, G. T., Mallia, A. K., Gartner, F. H., Provenzano, M. D., Fujimoto, E. K., Goeke, N. M., Olson, B. J., and Klenk, D. C. (1985) Measurement of Protein Using Bicinchoninic Acid, *Anal Biochem 150*, 76-85.

73. Callan, J. F., Mulrooney, R. C., and Kamila, S. (2008) Luminescent detection of ATP in aqueous solution using positively charged CdSe-ZnS quantum dots, *J Fluoresc 18*, 1157-1161.

74. Kong, C., Qin, L. X., Liu, J. F., Zhong, X. H., Zhu, L. Y., and Long, Y. T. (2010) Determination of dissolved oxygen based on photoinduced electron transfer from quantum dots to methyl viologen, *Analytical Methods 2*, 1056-1062.

75. George, S. J., Igarashi, R. Y., Xiao, Y., Hernandez, J. A., Demuez, M., Zhao, D., Yoda, Y., Ludden, P. W., Rubio, L. M., and Cramer, S. P. (2008) Extended X-ray absorption fine structure and nuclear resonance vibrational spectroscopy reveal that NifB-co, a FeMo-co precursor, comprises a 6Fe core with an interstitial light atom, *J Am Chem Soc 130*, 5673-5680.

76. Seefeldt, L. C., Morgan, T. V., Dean, D. R., and Mortenson, L. E. (1992) Mapping the site(s) of MgATP and MgADP interaction with the nitrogenase of Azotobacter vinelandii. Lysine 15 of the iron protein plays a major role in MgATP interaction, *J Biol Chem 267*, 6680-6688.

77. Lakowicz, J. R. (2006) *Principles of Fluorescence Spectroscopy*, 4 ed., Springer, New York.

78. Nozik, A. J. (2010) Nanoscience and nanostructures for photovoltaics and solar fuels, *Nano Lett 10*, 2735-2741.

79. Landes, C., Burda, C., Braun, M., and El-Sayed, M. A. (2001) Photoluminescence of CdSe nanoparticles in the presence of a hole acceptor: n-butylamine, *Journal of Physical Chemistry B 105*, 2981-2986.

80. Hagen, W. R. (2006) EPR spectroscopy as a probe of metal centres in biological systems, *Dalton Trans*, 4415-4434.

81. Frank, P., Angove, H. C., Burgess, B. K., and Hodgson, K. O. (2001) Determination of ligand binding constants for the iron-molybdenum cofactor of nitrogenase: monomers, multimers, and cooperative behavior, *J Biol Inorg Chem 6*, 683-697.

82. Barney, B. M., McClead, J., Lukoyanov, D., Laryukhin, M., Yang, T. C., Dean, D. R., Hoffman, B. M., and Seefeldt, L. C. (2007) Diazene (HN=NH) is a substrate for nitrogenase: insights into the pathway of N2 reduction, *Biochemistry 46*, 6784-6794.

83. Smith, B. E., Durrant, M. C., Fairhurst, S. A., Gormal, C. A., Gronberg, K. L. C., Henderson, R. A., Ibrahim, S. K., Le Gall, T., and Pickett, C. J. (1999) Exploring the reactivity of the isolated iron-molybdenum cofactor of nitrogenase, *Coord Chem Rev 185-6*, 669-687.

84. Barney, B. M., Lee, H. I., Dos Santos, P. C., Hoffman, B. M., Dean, D. R., and Seefeldt, L. C. (2006) Breaking the N2 triple bond: insights into the nitrogenase mechanism, *Dalton Trans*, 2277-2284.

85. Igarashi, R. Y., Laryukhin, M., Dos Santos, P. C., Lee, H. I., Dean, D. R., Seefeldt, L. C., and Hoffman, B. M. (2005) Trapping H- bound to the nitrogenase FeMo-cofactor active site during H2 evolution: characterization by ENDOR spectroscopy, *J Am Chem Soc 127*, 6231-6241.

86. Wuister, S. F., Swart, I., van Driel, F., Hickey, S. G., and Donega, C. D. (2003) Highly luminescent water-soluble CdTe quantum dots, *Nano Lett 3*, 503-507.

87. Han, H. Y., Sheng, Z. H., and Liang, H. G. (2006) A novel method for the preparation of water-soluble and small-size CdSe quantum dots, *Materials Letters 60*, 3782-3785.

88. Noh, M., Kim, T., Lee, H., Kim, C. K., Joo, S. W., and Lee, K. (2010) Fluorescence quenching caused by aggregation of water-soluble CdSe quantum dots, *Colloids and Surfaces a-Physicochemical and Engineering Aspects 359*, 39-44.

89. Rogach, A. L., Kornowski, A., Gao, M. Y., Eychmuller, A., and Weller, H. (1999) Synthesis and characterization of a size series of extremely small thiol-stabilized CdSe nanocrystals, *Journal of Physical Chemistry B 103*, 3065-3069.

90. Dyer, D. H., Rubio, L. M., Thoden, J. B., Holden, H. M., Ludden, P. W., and Rayment, I. (2003) The three-dimensional structure of the core domain of Naf Y from Azotobacter vinelandii determined at 1.8-A resolution, *J Biol Chem 278*, 32150-32156.

91. Mehta, S. K., Chaudhary, S., Kumar, S., and Singh, S. (2010) Facile synthesis, growth mechanism, and optical properties of CdSe nanoparticles in self-assembled micellar media and their efficient conjugation with proteins, *Journal of Nanoparticle Research 12*, 1697-1709.

92. Pickett, C. J., Vincent, K. A., Ibrahim, S. K., Gormal, C. A., Smith, B. E., and Best, S. P. (2003) Electron-transfer chemistry of the iron-molybdenum cofactor of nitrogenase: Delocalized and localized reduced states of FeMoco which allow binding of carbon monoxide to iron and molybdenum, *Chemistry-a European Journal 9*, 76-87.

93. Deistung, J., Cannon, F. C., Cannon, M. C., Hill, S., and Thorneley, R. N. (1985) Electron transfer to nitrogenase in Klebsiella pneumoniae. nifF gene cloned and the gene product, a flavodoxin, purified, *Biochem J 231*, 743-753.

94. Lee, C. C., Hu, Y., and Ribbe, M. W. (2012) ATP-Independent Formation of Hydrocarbons Catalyzed by Isolated Nitrogenase Cofactors, *Angew Chem Int Ed Engl 51*, 1947-1949.

95. Igarashi, R. Y., and Seefeldt, L. C. (2003) Nitrogen fixation: the mechanism of the Mo-dependent nitrogenase, *Crit. Rev. Biochem. Mol. Biol. 38*, 351-384.

96. Spatzal, T., Aksoyoglu, M., Zhang, L., Andrade, S. L. A., Schleicher, E., Weber, S., Rees, D. C., and Einsle, O. (2011) Evidence for interstitial carbon in nitrogenase FeMo cofactor, *Science (Washington, DC, U. S.) 334*, 940.

97. George, S. J., Igarashi, R. Y., Xiao, Y., Hernandez, J. A., Demuez, M., Zhao, D., Yoda, Y., Ludden, P. W., Rubio, L. M., and Cramer, S. P. (2008) Extended X-ray absorption fine structure and nuclear resonance vibrational spectroscopy reveal that NifB-co, a FeMo-co precursor, comprises a 6Fe core with an interstitial light atom, *J. Am. Chem. Soc. 130*, 5673-5680.

98. Hernandez, J. A., Igarashi, R. Y., Soboh, B., Curatti, L., Dean, D. R., Ludden, P. W., and Rubio, L. M. (2007) NifX and NifEN exchange NifB cofactor and the VK-cluster, a newly isolated intermediate of the iron-molybdenum cofactor biosynthetic pathway, *Mol. Microbiol. 63*, 177-192.

99. Rubio, L. M., Rangaraj, P., Homer, M. J., Roberts, G. P., and Ludden, P. W. (2002) Cloning and mutational analysis of the γ gene from *Azotobacter vinelandii* defines a new family of proteins capable of metallocluster binding and protein stabilization, *J. Biol. Chem. 277*, 14299-14305.

100. Lee, H.-I., Hales, B. J., and Hoffman, B. M. (1997) Metal-ion valencies of the FeMo cofactor in CO-inhibited and resting state nitrogenase by ^{57}Fe Q-band ENDOR, *J. Am. Chem. Soc. 119*, 11395-11400.

101. Bittner, F., and Mendel, R.-R. (2010) Cell biology of molybdenum, *Plant Cell Monogr. 17*, 119-143.

102. Mendel, R. R., Smith, A. G., Marquet, A., and Warren, M. J. (2007) Metal and cofactor insertion, *Nat. Prod. Rep. 24*, 963-971.

103. Mendel, R. R. (2005) Molybdenum: biological activity and metabolism, *Dalton Trans.*, 3404-3409.

104. Schwarz, G., Mendel, R. R., and Ribbe, M. W. (2009) Molybdenum cofactors, enzymes and pathways, *Nature (London, U. K.) 460*, 839-847.

105. Mouncey, N. J., Mitchenal, L. A., and Pau, R. N. (1995) Mutational analysis of genes of the mod locus involved in molybdenum transport, homeostasis, and processing in *Azotobacter vinelandii*, *J. Bacteriol. 177*, 5294-5302.

106. Kowalewski, B., Poppe, J., Demmer, U., Warkentin, E., Dierks, T., Ermler, U., and Schneider, K. Nature's polyoxometalate chemistry: X-ray structure of the Mo storage protein loaded with discrete polynuclear Mo-O clusters, *J. Am. Chem. Soc.*, DOI: 10.1021/ja303084n.

107. Hernandez, J. A., George, S. J., and Rubio, L. M. (2009) Molybdenum trafficking for nitrogen fixation, *Biochemistry 48*, 9711-9721.

108. Allen, R. M., Roll, J. T., Rangaraj, P., Shah, V. K., Roberts, G. P., and Ludden, P. W. (1999) Incorporation of molybdenum into the iron-molybdenum cofactor of nitrogenase, *J. Biol. Chem. 274*, 15869-15874.

109. Rangaraj, P., and Ludden, P. W. (2002) Accumulation of ^{99}Mo-containing iron-molybdenum cofactor precursors of nitrogenase on NifNE, NifH, and NifX of *Azotobacter vinelandii*, *J. Biol. Chem. 277*, 40106-40111.

110. Strandberg, G. W., and Wilson, P. W. (1968) Formation of the nitrogen-fixing enzyme system in *Azotobacter vinelandi*i, *Can. J. Microbiol. 14*, 25-32.

111. Sen, S., Igarashi, R., Smith, A., Johnson, M. K., Seefeldt, L. C., and Peters, J. W. (2004) A conformational mimic of the MgATP-bound "on state" of the nitrogenase iron protein, *Biochemistry 43*, 1787-1797.

112. Soboh, B., Igarashi, R. Y., Hernandez, J. A., and Rubio, L. M. (2006) Purification of a NifEN protein complex that contains bound molybdenum and a FeMo-Co precursor from an *Azotobacter vinelandii* ΔnifHDK strain, *J. Biol. Chem. 281*, 36701-36709.

113. Burgess, B. K., Jacobs, D. B., and Stiefel, E. I. (1980) Large-scale purification of high activity *Azotobacter vinelandii* nitrogenase, *Biochim. Biophys. Acta, Enzymol. 614*, 196-209.

114. Paschinger, H. (1974) Changed nitrogenase activity in *Rhodospirillum rubrum* after substitution of tungsten for molybdenum, *Arch. Microbiol. 101*, 379-389.

115. Higgins, E. S., Richert, D. A., and Westerfeld, W. W. (1956) Tungstate antagonism of molybdate in *Aspergillus niger*, *Proc. Soc. Exp. Biol. Med. 92*, 509-511.

116. Benemann, J. R., Smith, G. M., Kostel, P. J., and McKenna, C. E. (1973) Tungsten incorporation into *Azotobacter vinelandii* nitrogenase, *FEBS Lett. 29*, 219-221.

117. Bulen, W. A. (1961) Effect of tungstate on the uptake and function of molybdate in *Azotobacter agilis*, *J. Bacteriol. 82*, 130-134.

118. Lawson, D. M., Williams, C. E. M., Mitchenall, L. A., and Pau, R. N. (1998) Ligand size is a major determinant of specificity in periplasmic oxyanion-binding proteins: the 1.2 Å resolution crystal structure of *Azotobacter vinelandii* ModA, *Structure (London, U.K.) 6*, 1529-1539.

119. Siemann, S., Schneider, K., Oley, M., and Mueller, A. (2003) Characterization of a tungsten-substituted nitrogenase isolated from *Rhodobacter capsulatus*, *Biochemistry 42*, 3846-3857.

120. Hales, B. J., and Case, E. E. (1987) Nitrogen fixation by *Azotobacter vinelandii* in tungsten-containing medium, *J. Biol. Chem. 262*, 16205-16211.

121. Hu, Y., Corbett, M. C., Fay, A. W., Webber, J. A., Hodgson, K. O., Hedman, B., and Ribbe, M. W. (2006) FeMo cofactor maturation on NifEN, *Proc. Natl. Acad. Sci. U. S. A. 103*, 17119-17124.

122. Yoshizawa, J. M., Blank, M. A., Fay, A. W., Lee, C. C., Wiig, J. A., Hu, Y., Hodgson, K. O., Hedman, B., and Ribbe, M. W. (2009) Optimization of FeMoco maturation on NifEN, *J. Am. Chem. Soc. 131*, 9321-9325.

123. Hu, Y., Fay, A. W., and Ribbe, M. W. (2005) Identification of a nitrogenase FeMo cofactor precursor on NifEN complex, *Proc. Natl. Acad. Sci. U. S. A. 102*, 3236-3241.

124. Yoshizawa, J. M., Fay, A. W., Lee, C.-C., Hu, Y., and Ribbe, M. W. (2010) Insertion of heterometals into the NifEN-associated iron-molybdenum cofactor precursor, *J. Biol. Inorg. Chem. 15*, 421-428.

125. Lanzilotta, W. N., Ryle, M. J., and Seefeldt, L. C. (1995) Nucleotide hydrolysis and protein conformational changes in *Azotobacter vinelandii* nitrogenase iron protein: defining the function of aspartate-129, *Biochemistry 34*, 10713-10723.

126. Barber, M. J., Coughlan, M. P., Rajagopalan, K. V., and Siegel, L. M. (1982) Properties of the prosthetic groups of rabbit liver aldehyde oxidase: a comparison of molybdenum hydroxylase enzymes, *Biochemistry 21*, 3561-3568.

127. Barber, M. J., and Siegel, L. M. (1982) Oxidation-reduction potentials of molybdenum, flavin, and iron-sulfur centers in milk xanthine oxidase: variation with pH, *Biochemistry 21*, 1638-1647.

128. Shannon, R. D. (1976) Revised effective ionic radii and systematic studies of interatomic distances in halides and chalcogenides, *Acta Crystallogr., Sect. A A32*, 751-767.

129. Hagedoorn, P.-L., Hagen, W. R., Stewart, L. J., Docrat, A., Bailey, S., and Garner, C. D. (2003) Redox characteristics of the tungsten DMSO reductase of *Rhodobacter capsulatus*, *FEBS Lett. 555*, 606-610.

130. George, S. J., Igarashi, R. Y., Piamonteze, C., Soboh, B., Cramer, S. P., and Rubio, L. M. (2007) Identification of a Mo-Fe-S cluster on NifEN by Mo K-edge extended X-ray absorption fine structure, *J. Am. Chem. Soc. 129*, 3060-3061.

131. Corbett, M. C., Hu, Y., Fay, A. W., Ribbe, M. W., Hedman, B., and Hodgson, K. O. (2006) Structural insights into a protein-bound iron-molybdenum cofactor precursor, *Proc. Natl. Acad. Sci. U. S. A. 103*, 1238-1243.

132. Kaiser, J. T., Hu, Y., Wiig, J. A., Rees, D. C., and Ribbe, M. W. (2011) Structure of precursor-bound NifEN: a nitrogenase FeMo cofactor maturase/insertase, *Science (Washington, DC, U. S.) 331*, 91-94.

133. Yu, W. W., Wang, Y. A., and Peng, X. G. (2003) Formation and stability of size-, shape-, and structure-controlled CdTe nanocrystals: Ligand effects on monomers and nanocrystals, *Chemistry of Materials 15*, 4300-4308.

134. Kudo, A. (2011) Periostin in fibrillogenesis for tissue regeneration: periostin actions inside and outside the cell, *Cellular and Molecular Life Sciences 68*, 3201-3207.

135. Zhu, H., Song, N., and Lian, T. (2010) Controlling charge separation and recombination rates in CdSe/ZnS type I core-shell quantum dots by shell thicknesses, *J Am Chem Soc 132*, 15038-15045.

136. Nozik, A. J., Beard, M. C., Luther, J. M., Law, M., Ellingson, R. J., and Johnson, J. C. (2010) Semiconductor Quantum Dots and Quantum Dot Arrays and Applications of Multiple Exciton Generation to Third-Generation Photovoltaic Solar Cells, *Chem Rev 110*, 6873-6890.

137. Thorneley, R. N., and Lowe, D. J. (1984) The mechanism of Klebsiella pneumoniae nitrogenase action. Pre-steady-state kinetics of an enzyme-bound intermediate in N2 reduction and of NH3 formation, *Biochem J 224*, 887-894.

138. Mayhew, S. G. (1978) The redox potential of dithionite and SO-2 from equilibrium reactions with flavodoxins, methyl viologen and hydrogen plus hydrogenase, *Eur J Biochem 85*, 535-547.

139. Cleland, W. W. (1964) Dithiothreitol, a New Protective Reagent for Sh Groups, *Biochemistry 3*, 480-482.

140. Millis, K. K., Weaver, K. H., and Rabenstein, D. L. (1993) Oxidation-Reduction Potential of Glutathione, *Journal of Organic Chemistry 58*, 4144-4146.

141. Hagen, W. R., Dunham, W. R., Braaksma, A., and Haaker, H. (1985) On the prosthetic group(s) of component II from nitrogenase. EPR of the Fe-protein from Azotobacter vinelandii, *FEBS Lett 187*, 146-150.

142. Ryle, M. J., Lanzilotta, W. N., and Seefeldt, L. C. (1996) Elucidating the mechanism of nucleotide-dependent changes in the redox potential of the [4Fe-4S] cluster in nitrogenase iron protein: the role of phenylalanine 135, *Biochemistry 35*, 9424-9434.